AEDC-TR-71-186

cy.2

DEC 6 1971

AUG 14 1989


# CALCULATION OF FORCES ON AIRCRAFT STORES LOCATED IN DISTURBED FLOW FIELDS FOR APPLICATION IN STORE SEPARATION PREDICTION

W. N. MacDermott and P. W. Johnson
ARO, Inc.

November 1971

Approved for public release; distribution unlimited.

PROPULSION WIND TUNNEL FACILITY
ARNOLD ENGINEERING DEVELOPMENT CENTER
AIR FORCE SYSTEMS COMMAND
ARNOLD AIR FORCE STATION, TENNESSEE

PROPERTY OF U S AIR FORCE
AEDC LIBRARY
F40600-72-C-0003

# NOTICES

When U. S. Government drawings specifications, or other data are used for any purpose other than a definitely related Government procurement operation, the Government thereby incurs no responsibility nor any obligation whatsoever, and the fact that the Government may have formulated, furnished, or in any way supplied the said drawings, specifications, or other data, is not to be regarded by implication or otherwise, or in any manner licensing the holder or any other person or corporation, or conveying any rights or permission to manufacture, use, or sell any patented invention that may in any way be related thereto.

Qualified users may obtain copies of this report from the Defense Documentation Center.

References to named commercial products in this report are not to be considered in any sense as an endorsement of the product by the United States Air Force or the Government.

# CALCULATION OF FORCES ON AIRCRAFT STORES LOCATED IN DISTURBED FLOW FIELDS FOR APPLICATION IN STORE SEPARATION PREDICTION

W. N. MacDermott and P. W. Johnson
ARO, Inc.

Approved for public release; distribution unlimited.

## FOREWORD

The work reported herein was sponsored by the Air Force Armament Laboratory (AFATL), Air Force Systems Command (AFSC), under Program Element 63716F, System 670A. Technical monitor for AFATL was Capt. Victor E. Studwell.

The results of this research were obtained by ARO, Inc. (a subsidiary of Sverdrup & Parcel and Associates, Inc.), contract operator of the Arnold Engineering Development Center (AEDC), AFSC, Arnold Air Force Station, Tennessee, under Contract F40600-72-C-0003. The work was performed from April 1, 1970, through June 30, 1971, under ARO Projects PW5080 and PW5180. The manuscript was submitted for publication on August 6, 1971.

This technical report has been reviewed and is approved.

| | |
|---|---|
| Maurice A. Clermont | Robert O. Dietz |
| Captain, CF | Acting Director |
| Research & Development Div. | Directorate of Technology |
| Directorate of Technology | |

## ABSTRACT

The aerodynamic characteristics of an M-117 bomb in steady, incompressible, potential flow are computed by representing the bomb planform with a discrete network of vortex singularities. Distribution of velocity and pressure coefficients over the bomb, as well as total force and moment coefficients, are calculated as functions of pitch attitude, the surrounding flow field, and various assumed vortex-lattice modelings. Both spatially uniform and nonuniform flow fields are investigated; the nonuniformities were created by the presence of a parent aircraft. For a properly modeled bomb immersed in a uniform flow, the lift and pitching moment coefficients summed over the entire configuration are found to be within 10 percent of wind tunnel measurements. When the bomb is surrounded by the disturbance flow field produced by an F-4C aircraft, the incremental effects on lift and pitching moment are very similar for theory and experiment.

## CONTENTS



## APPENDIX
## ILLUSTRATIONS

Figure

## NOMENCLATURE

| | |
|---|---|
| A/C | Aircraft |
| $B_x$, $B_y$, $B_z$ | Direction cosines of unit normal at boundary points |
| $C_A$ | Axial-force coefficient |
| $C_D$ | Drag coefficient |
| $C_{D_o}$ | Drag coefficient at $\alpha$ = 0 deg |
| $(C_D)_{fric}$ | Skin-friction drag coefficient |
| $C_L$ | Lift coefficient |
| $C_{L'}$ | Local lift coefficient |
| $C_m$ | Pitching-moment coefficient about center of gravity |
| $C_p$ | Pressure coefficient defined by Eqs. (23) and (24) |
| $C_{p_i}$ | Pressure coefficient of internal flow |
| $C_{p_b}$ | Base pressure coefficient |
| c | Reference length, 4.395 in. |
| $\vec{F}$ | Aerodynamic force |
| $\vec{G}$ | Geometric influence coefficient defined by Eq. (14) |
| H | Matrix of geometric factors defined by Eq. (18) |
| M | Mach number |
| NUFF | Nonuniform flow field |
| $\vec{n}$ | Unit vector normal to surface |
| p | Static pressure |
| q | Dynamic pressure |
| $S_{base}$ | Base area of bomb, 0.2241 $in.^2$ |
| $S_{ref}$ | Reference area, 0.5025 $in.^2$ |
| $S_{wet}$ | Effective wetted area of bomb, 9.912 $in.^2$ |
| $\vec{U}_\infty$ | Velocity in the flow field surrounding a store |
| $\vec{V}$ | Velocity defined by Eq. (4) |
| $\Delta\vec{V}$ | Velocity resulting from distributed vorticity contribution |
| X, Y, Z | Coordinates in parent aircraft reference system |

| | |
|---|---|
| x, y, z | Coordinates in store reference system |
| $\alpha$ | Angle of attack, positive nose up |
| $\Delta\alpha_o$ | Angle of attack for $C_L = 0$ |
| $\vec{\Gamma}$ | Net vorticity strength on a segment of a vortex filament |
| $\Gamma$ | Magnitude of $\vec{\Gamma}$ |
| $\theta_D$ | Downwash angle, positive downward |
| $\rho$ | Density |

## SUBSCRIPTS

| | |
|---|---|
| i | Straight line segment of a horseshoe vortex |
| j | Horseshoe vortex |
| k | Field point at which velocity is calculated |
| $\infty$ | Free-stream condition |

## OTHER

| | |
|---|---|
| $[F_x, F_y, F_z]$ | Alternate notation for any vector $\vec{F}$ with components $F_x$, $F_y$, $F_z$ |

# SECTION I
# INTRODUCTION

Adverse or critical store separation characteristics are usually not determined until quite late in the development of a given weapons system because higher priority is usually assigned in wind tunnel programs to areas affecting performance of the parent aircraft itself and because of the lack of any analytical methods of predicting store separation trajectories in the nonuniform flow fields existing beneath parent aircraft. Another factor militating against comprehensive store separation testing early in the development stage is the sheer volume of testing required to cover all of the many possible combinations of stores on a given aircraft. Furthermore, many stores are not even developed until the aircraft is well into its service life, and store separation testing frequently continues into this stage in both flight and wind tunnel testing.

It is recognized that any analytical assistance in store separation analysis would be of appreciable value to both wind tunnel tests and flight tests. Not only could wind tunnel tests be planned more intelligently, by screening out clearly noncritical cases, but analytical methods could be used to conduct parametric variations about "base" cases measured in the wind tunnel. In addition, theoretical techniques would be of value in analysis of critical cases discovered in flight or in the wind tunnel.

Under a previous project, a complete set of measurements of the nonuniform flow field beneath a 1/20-scale F-4C aircraft model was obtained for four different store combinations. The force coefficients on a model of the M-117 bomb were also measured at different locations in these nonuniform flow fields and in uniform flow. These data (some 12,000 data points) were intended to provide basic information for study of analytical techniques. Initially, it was envisioned that the present research effort would be composed of three parts: a theoretical calculation of force coefficients on the M-117 bomb in the F-4C flow field for comparison with measured values, an empirical correlation of the measured force coefficients in sufficient generality for use in store separation calculations, and an application of the more successful of these two approaches to actual store separation trajectory calculations. As it has developed, the main part of this research effort has been concentrated on the theoretical calculation of force coefficients of the M-117 bomb. It was not found possible to obtain a generally satisfactory correlation of the experimental force coefficients, and no attempts at trajectory calculations were made.

## SECTION II
## GENERAL DESCRIPTION OF STORE SEPARATION PREDICTION

The trajectory of a freely falling store separating from a parent aircraft can be calculated by a double integration of the equations of motion

$$\text{Trajectory} = T(t) = X_i(t) = \iint \frac{F_i}{m}\, dt\, dt + C_1 t + C_2 \quad i = 1,2,3 \qquad (1)$$

Clearly, the trajectory has a functional dependence on the initial conditions, the store inertia, and the aerodynamic forces on the store. These, in turn, depend upon numerous other parameters

$$\left.\begin{aligned} &\text{Initial conditions} = f(\text{separation force, location of carriage position on aircraft}) \\ &\text{Inertial character of store} = f(\text{mass, center of gravity location}) \\ &\text{Store forces} = f(M_\infty, \text{altitude, store shape, parent aircraft configuration, aircraft attitude in flight, relative orientation of aircraft and store}) \end{aligned}\right\} \qquad (2)$$

It is noted that Eq. (1) is only the integration of linear momentum and that integration of angular momentum equations would also be required because of influence of store angular orientation on the store forces.

In any analytical calculation of store separation trajectories by means of Eq. (1), the key part of the calculation will be the aerodynamic forces on the store, $F_i$, and the source of these force characteristics will define the method used. The difficulty in obtaining the store forces is that the store is immersed in a nonuniform flow field (NUFF), produced by the parent aircraft, at least near the critical initial stages of the trajectory. This means that in addition to the usual dependence on attitude, store force will also depend upon spatial position with respect to the aircraft, that is, $F_i(X, Y, Z, \text{attitude})$. If this spatial dependence were not present, special store separation tests in the wind tunnel would not even be necessary. It would be sufficient to measure the store force coefficients in uniform flow with no parent aircraft present and to use these coefficients as inputs for integration of the equations of motion.

## 2.1 EXPERIMENTAL METHOD

The most straightforward source of store force characteristics is experiment. The store force coefficients are measured in a wind tunnel at a large number of points in a three-dimensional grid beneath a model of the parent aircraft, $F_i(X, Y, Z, \text{attitude})$. These data are stored in an array and, using three-dimensional interpolation, used as input to a numerical integration procedure which is almost always performed in a large digital computer. This method has become known as the "grid method." It is probably quite accurate but requires a large amount of wind tunnel test time if more than a single aircraft-store combination is to be studied. If only a single combination is of interest, however, it is adaptable to a parametric study which includes altitude, separation force, carriage location, store mass and center of gravity. Parameters which cannot be varied systematically entirely on the computer are Mach number, aircraft configuration, store configuration, and aircraft attitude. So far, the grid method has been limited to planar trajectories.

The Captive Trajectory System (CTS) used in the AEDC-PWT Aerodynamic Wind Tunnel (4T) can be recognized as a special form of this experimental method. The force grid is not acquired in toto from the wind tunnel, but force coefficients are obtained only at a sequence of closely spaced points along any given trajectory. The wind tunnel is used as a source of aerodynamic data and in a closed loop with a digital computer which integrates the equation of motion point-by-point and positions the model in the tunnel at the sequence of points predicted by this integration. Generally, the same parametric variation can be made in a CTS test as in a grid method calculation. The disadvantage is, of course, that the calculation inherently requires wind tunnel operation; the advantage is that aerodynamic data need be measured only along store trajectories.

## 2.2 THEORETICAL METHOD

It is of interest to investigate analytic means by which the force characteristics can be obtained short of complete reliance on wind tunnel tests. It is possible to obtain the exact solution for the flow field (and hence forces) over a parent aircraft and a separating store for any relative orientation of the two bodies in an incompressible, inviscid flow. In compressible flow, the differential equation of the velocity potential is highly nonlinear and exact solutions are not generally possible to obtain. Almost all work in the compressible regime is done in the linearized approximation. Some attempts to calculate store forces in this approximation have been made (Ref. 1) but in the present

case, it was desired to retain the accuracy of exact incompressible solutions. In this case, the calculation of the flow field requires a solution of the Laplace equation

$$\nabla^2 \Phi = 0 \tag{3}$$

subject to the Neumann boundary condition on each body

$$\text{grad } \Phi \cdot \vec{n} = -\vec{V} \cdot \vec{n} = 0 \tag{4}$$

and the boundary condition at infinity

$$\text{grad } \Phi = -\vec{U}_\infty \text{ at } X=Y=Z=\infty \tag{5}$$

Since the Laplace equation is linear, superposition of elementary solutions (sources, sinks, and vortices) will allow buildup of a complex flow which satisfies the boundary conditions, Eqs. (4) and (5), with no restrictions on body thickness.

Although the procedure just outlined is straightforward in principle, in practice it can represent a prodigious calculation problem, even on a modern large capacity computer. Although most aircraft stores are geometrically simple shapes which can be represented by a relatively small number of elementary flow solutions (singularities), the parent aircraft is usually a quite complex shape and the combined solution for both aircraft and store could require of the order of 1000 elementary solutions. In addition to the mathematical processing and "bookkeeping" associated with this many singularities, the crux of such a flow calculation is the solution of a system of linear algebraic equations equal in number and in number of unknowns to this number of singularities. A solution of this order of complexity might require many hours on even a large digital computer. When it is further considered that such a lengthy solution would provide the store forces at only one point on a trajectory, the possibility of such an approach to store separation prediction is clearly seen to be a practical impossibility.

## 2.3 PRACTICAL HYBRID METHOD

Further analysis suggests that there are conditions of relative separation of aircraft and store for which the required number of singularities can be reduced to manageable proportions.

### 2.3.1 Regimes of Interference of Two Bodies

It is recognized that when two bodies are of appreciably different size, as is the case for an aircraft and a store, there are three possible

regimes of relative orientation of the two shapes. For generally small separation, the disturbance field produced by each body extends to the other body, Fig. 1a, Appendix. In other words, the perturbation potentials resulting from each body are significant at the other body. This is the classic case of mutual interference for which the potential flow problem represented by Eqs. (3) through (5) must be solved simultaneously for both bodies, leading to excessive computer requirements.

However, there is an intermediate range of separation of the two bodies for which the perturbation of the smaller body will be negligible at the larger body, Fig. 1b, the case of simple interference of the large body on the small body. In a mathematical sense, this allows a certain simplification of the problem since the flow over the larger body can be obtained without regard to the boundary conditions on the smaller body and this flow can then subsequently be used to provide nonuniform flow boundary conditions for a solution of the smaller body flow. The actual reduction of computer requirements, however, would not be great because the main contribution to the number of singularities required in the full solution is in the parent aircraft simulation.

There is, of course, the trivial case, Fig. 1c, in which separation of the two bodies is such that there is no interference of any kind and the flow over either could be calculated without reference to the other body.

### 2.3.2 Possible Hybrid Method for Simple Interference Regime

In the intermediate regime of simple interference, the NUFF produced by the parent aircraft is all that is required for boundary conditions for a potential flow calculation on the store alone. As a result of this decoupling of the store flow solution from the parent aircraft flow solution, several possibilities present themselves. A potential flow over the parent aircraft could still be calculated to provide $(NUFF)_{A/C}$ with the result that the larger of the two potential flow calculations would then be appreciably smaller than for the two-body case. However, the tremendous advantage to be gained by performing potential flow calculations for only the store suggests the possibility of obtaining the $(NUFF)_{A/C}$ from experimental measurements rather than from a potential flow calculation. This is, in fact, the approach followed in the present study, using the flow-field measurements of a previous project.

The nature of the elementary singularities used to construct the store is such that the boundary condition at infinity is automatically

satisfied and the condition at the surface of the store itself, Eq. (4), must be modified to reflect a NUFF

$$\vec{V}\cdot\vec{n} = (\vec{U}_{\infty}(x,y,z) + \vec{U}_{\text{singularities}}) \cdot \vec{n} = 0 \qquad (6)$$

where the $(\text{NUFF})_{A/C}$ is given by $\vec{U}_{\infty}(x, y, z)$. There are actually two very great advantages to be gained from performing potential flow calculations for the store only:

1. The magnitude of the potential flow problem to be solved by the method of singularities can be reduced to a more practical level of 100 to 200 singularities.
2. Of equal importance, as a result of reduction to a single-body problem, the main part of the potential flow solution (calculation of the influence coefficients and inversion of the coefficient matrix of the system of simultaneous linear equations) need be done only one time for a given store. Completion of the solution for any set of boundary conditions (different NUFF or orientation of the store within the NUFF) becomes a very small matter for a modern computer, Section 3. 3. As an example, once the main part of the potential flow problem for a given store shape has been obtained, which might require up to an hour of computing time, subsequent completion of the solution for specific boundary conditions at any trajectory point might require only 3 min per point on an IBM 360/50 computer. Such computing requirements are no longer classifiable as prohibitive and certainly justify a careful evaluation of the merits of this proposed calculation.

### 2.3.3 Inherent Approximations of the Proposed Hybrid Method

In a proposed method of calculation of store forces by means of an "exact" potential flow solution for the store, using the NUFF boundary conditions measured in a wind tunnel test for a given parent aircraft, there are a number of effects which represent inherent approximations in this method which should be kept in mind for subsequent evaluation:

1. Compressibility Effects

   The potential flow solutions are necessarily performed for the incompressible flow case. At the Mach numbers of interest, there will be compressibility effects which can be allowed for by the usual linearized rules (Goethert, Prandtl-Glauert), but

these rules are approximations which lose accuracy for bodies of the thickness ratio of the M-117 bomb. It may turn out that experimental data are a more valuable source of compressibility corrections.

2. Viscous Effects

   Since the potential flow solutions do not include viscous forces, a correction to the axial force should be evaluated, based on wind tunnel measurement or a skin-friction calculation. This is fairly straightforward, but second-order effects of viscosity are not. By these are meant the shedding of trailing vortices from the lee side of the bomb body at nonzero angle of attack, resulting in nonlinear force coefficients. The angle of attack at which such vortex shedding occurs (and changes the entire flow pattern) is not known.

3. Mutual Interference Effects

   As noted, the proposed method completely ignores the effects of mutual interference between the parent aircraft and the store - that is, small separations of the order of a single store diameter. Evaluation of such effects was beyond the scope of this investigation. It is possible, for sufficiently energetic separation forces, that the time of residence of the store in the mutual interference regime is so short that the effects on the trajectory are negligible. In any event, the practical analytical method outlined in Section 2.3.2 cannot include this effect so that it could only be allowed for by an empirical correction.

## 2.4 PARAMETRIC CAPABILITY OF THEORETICAL METHODS

The parametric capability of the completely theoretical approach would be unlimited, albeit at the expense of gargantuan computer requirements. In the suggested "practical" method, however, which substitutes an experimentally determined $(NUFF)_{A/C}$ for a calculated one, all parameters can be varied in the computing routines except the parent aircraft configuration and its attitude. Any variation of these parameters would require a new measurement of a different $(NUFF)_{A/C}$ in each case.

# SECTION III
# DESCRIPTION OF ANALYTICAL DETERMINATION OF STORE FORCES BY THE VORTEX-LATTICE METHOD

Potential flow solutions in the incompressible case can be constructed to any degree of complexity by superposition of elementary solutions for sources, sinks, doublets, and vortices. Since each of these solutions represents a singularity in the flow, this method is often referred to as the method of singularities. The Douglas Neumann Program, Ref. 2, is a good example of a method involving only sources and sinks. This program is inadequate for bodies which incorporate three-dimensional lifting surfaces because neither sources nor sinks can represent trailing vorticity in the flow. In such cases, vortex elements must also be considered as elementary solutions. The Boeing Company has developed a very comprehensive potential flow program, Ref. 3, which was found to exceed the normal capacity of the IBM 360/50 computer, but which incorporates vortices as well as sources and sinks as the elementary solutions. Since no program was available which had the required capability for the present purposes, a new potential flow program was developed, based on use of vortices alone.

## 3.1 FUNDAMENTALS OF VORTEX REPRESENTATION OF A SOLID BODY

For various reasons it is important to consider the physical meaning of the vortex-lattice representation of a physical body in a flow. This requires consideration of Prandtl's concepts of free and bound vorticity as described in Ref. 4. Prandtl noted that the presence of a solid body in a flow, Fig. 2a, created difficulties in calculation of velocities produced by a vortex system. It was proposed to regard the body as nonsolid, with the volume contained within the surface contour filled with fluid, rendering the fluid region to be simply connected and allowing the vortex field relations valid for regions of infinite extent to be applied. The fluid inside the defining contour was assumed to be at rest at a pressure equal to the stagnation point pressure. Thus, there was at the surface of the body a velocity discontinuity which was considered an infinitely thin vortex sheet. Thus, any solid body is completely equivalent in external flow to a sheet of continuously distributed vorticity at the location of the surface of the body, Fig. 2b. The vorticity representing the solid body (the "bound" vorticity) does not obey the Helmholtz theorem on vortex motions since it is constrained to remain on the body surface. Prandtl further derived a conservation of vorticity such that wherever there was a variation in strength of bound vorticity, free vorticity was shed from the body and trailed downstream to infinity - the foundation of finite wing theory.

It is necessary for computational reasons to replace the distributed vortex sheet representation of a solid body (an exact concept) with a series of concentrated vortex elements having the same net strength (an approximation), Fig. 2c. This is because there are no general closed form expressions relating induced velocities to elements of distributed vorticity, but there are such simple expressions for elements of concentrated vorticity.

## 3.2 VORTEX FIELD RELATIONS

The superposition of vortex elements in a region of fluid flow may be considered as imposing a sort of "inner boundary condition," with the flow in the rest of the field being determined by the Laplace equation, $\nabla^2 \Phi = 0$. A relation exists between the incremental velocity at any point and the strength and orientation of the vortex element which is identical with the Biot-Savart law which describes the magnetic field induced by an electric current flowing through a conductor. By analogy, therefore, the flow-field velocity increment is referred to as the velocity "induced" by the vortex element, even though a direct physical mechanism relating the two is not obvious.

In its fluid-mechanical formulation, the Biot-Savart law is

$$d\vec{q}_P = \frac{\Gamma}{4\pi R^3} \; d\vec{s} \times \vec{R} \tag{7}$$

where $d\vec{q}_P$ is the induced velocity at point P induced by the vortex element $d\vec{s}$ having a strength $\Gamma$, and $\vec{R}$ is the radius vector from segment $d\vec{s}$ to the field point P. The entire vortex-lattice method is based on application of an integral of this simple equation.

For a finite length linear vortex element the total induced velocity at a field point P is found by integration of Eq. (7) to be

$$\vec{q}_P = \vec{P} \frac{\Gamma}{4\pi r} (\cos \theta_1 - \cos \theta_2) \; . \tag{8}$$

where r is the perpendicular distance from P to the vortex line, $\theta_1$ and $\theta_2$ are the angles between the vortex line and radius vectors from its end points to P, and $\vec{P}$ is a unit vector parallel to $d\vec{s} \times \vec{R}$, that is, perpendicular to the plane formed by the vortex element and the field point, Fig. 3.

There are occasions in dealing with trailing vorticity in which the velocity induced by a semi-infinite linear vortex element is required. In this case, integration of Eq. (7) gives

$$\vec{q}_p = \vec{P} \frac{\Gamma}{4\pi r} (1 - \cos \theta_2) \tag{9}$$

where the semi-infinite element is considered to be formed by allowing Point 1 of Fig. 3 to recede to infinity.

The unit vector $\vec{P}$ is readily evaluated from the vector $\vec{L} \times \vec{R}_1$ (or $\vec{L} \times \vec{R}_2$) as

$$\vec{P} = \frac{\vec{L}x\vec{R}_1}{|\vec{L}x\vec{R}_1|} = \frac{[a,b,c]}{\sqrt{a^2+b^2+c^2}} \tag{10}$$

where a, b, c are the components of the vector product $\vec{L} \times \vec{R}_1$ using the notation of Ref. 6. The perpendicular distance, r, is given as

$$r = \frac{|\vec{L}x\vec{R}_2|}{|\vec{L}|} \tag{11}$$

Since the components of the three vectors, $\vec{L}$, $\vec{R}_1$, and $\vec{R}_2$, are simply differences in the three cartesian coordinates of the three points in space, 1, 2, and P, it is clear that all of the vector relationships in Eqs. (8) through (10) contain a purely geometric component independent of the vortex element strength.

### 3.3 VORTEX-LATTICE METHOD

Although the surface vortex elements are usually arranged in a series of generally quadrilateral elements, Fig. 4a, it is convenient for calculational purposes to conceive of this array as being composed of a series of overlapping, adjacent horseshoe vortices, Fig. 4b. Each of the individual horseshoe vortices has a single spanwise element and an even number of generally chordwise segments, the last two of which are semi-infinite segments which trail downstream to infinity, Fig. 4c. The induced velocity at any field point, $P_k$, attributable to a single complete horseshoe vortex denoted by j is, of course, a summation of contributions of each of the i linear segments of the j horseshoe

$$\vec{q}_{k,j} = \sum_{i=1}^{N_j} \Gamma_j \left[\vec{P} \frac{(\cos \theta_1 - \cos \theta_2)}{4\pi r}\right]_{k,j,i} \tag{12}$$

Of course, corresponding to the two semi-infinite segments of the j-vortex, two of the terms of the summation of Eq. (12) will be of the form of Eq. (9); that is, with either $\cos \theta_1$ or $\cos \theta_2$ equal to unity. It is noted that the vortex strength is not involved in the summation, so that the entire induced velocity at k due to vortex j can be expressed in terms of a strength factor, $\Gamma_j$, times a geometric factor which depends on the orientation of j and k

$$\vec{q}_{k,j} = \Gamma_j \vec{G}_{k,j} \tag{13}$$

where $\vec{G}_{k,j}$ is the geometric influence coefficient

$$\vec{G}_{k,j} = \sum_{i=1}^{N_j} \left[ \vec{P} \frac{(\cos \theta_1 - \cos \theta_2)}{4\pi r} \right]_{k,j,i} \tag{14}$$

a vector quantity.

Clearly, if the strength of all the horseshoe vortices in the network, $\Gamma_j$, were known, the flow field would be completely determined because the velocity at any point in the field[1] could be calculated as the vector sum of $\vec{U}_\infty$ and all the induced velocities, $\vec{q}_{k,j}$

$$\vec{V}_k = \vec{U}_\infty + \sum_{j=1}^{N_j} \vec{q}_{k,j} = \vec{U}_\infty + \sum_{j=1}^{N_j} \vec{G}_{k,j} \Gamma_j \tag{15}$$

The unknowns, $\Gamma_j$, are determined by application of boundary conditions constraining the flow to be directed in a prescribed manner. The streamlines on the body are required to be tangential to the surface, and in addition (this is an optional capability), the streamtube they comprise may be constrained to any assumed direction near the forward and/or aft edges of a body. This requirement is imposed at a number of points exactly equal to the number of unknowns, $\Gamma_j$, such that a solvable system of linear equations results. The points at which the flow is constrained to be parallel to the surface are referred to as boundary points. A single boundary condition is expressed as

$$\vec{V}_k \cdot \vec{n}_k = (\vec{U}_\infty + \sum_{j=1}^{N_j} \vec{G}_{k,j} \Gamma_j) \cdot \vec{n}_k = 0 \tag{16}$$

which can be recognized as Eq. (4) written at a specific point. The

[1]This is not strictly true, as shown in Section 3.4.

system of $N_j$ equations representing all the required boundary conditions is thus

$$\sum_{j=1}^{N_j} (\vec{n}_k \cdot \vec{G}_{k,j})\Gamma_j = - (\vec{n}_k \cdot \vec{U}_{\infty_k}) \quad k = 1,\ldots,N_j \tag{17}$$

It is convenient to introduce the matrix notation

$$\left[H_{k,j}\right] = \left[\vec{n}_k \cdot \vec{G}_{k,j}\right] \tag{18}$$

giving

$$\left[H_{k,j}\right]\left\{\Gamma_j\right\} = \left\{- \vec{n}_k \cdot \vec{U}_{\infty_k}\right\} \tag{19}$$

as the system of equations to be solved for the elementary vortex strength, $\Gamma_j$. Each element of the H matrix is a scalar product of the unit normal to the surface at the boundary point and the geometric influence coefficient at k attributable to one of the individual horseshoe vortices, that is, the normal component of the geometric influence coefficient at the boundary point. Each row of the H matrix corresponds to a given boundary point. If the components of the unit normals are given in terms of the direction cosines of the normals

$$\vec{n}_k = \left[B_{x_k}, B_{y_k}, B_{z_k}\right] \tag{20}$$

then the H-matrix elements are given by

$$\left[H_{k,j}\right] = \left[B_{x_k} G_{x_{k,j}} + B_{y_k} G_{y_{k,j}} + B_{z_k} G_{z_{k,j}}\right] \tag{21}$$

The solution to the system of Eq. (19) can be expressed in terms of the inverse H matrix

$$\left\{\Gamma_j\right\} = \left[H_{k,j}\right]^{-1} \left\{-\vec{n}_k \cdot \vec{U}_{\infty_k}\right\}$$

Since the H matrix is purely geometric, depending only upon the shape of the vortex network and the location of the boundary points, the H-inverse matrix will also be purely geometrical. Once $\left[H_{k,j}\right]^{-1}$ has been obtained and stored in some readily available form, the flow field

in terms of $\Gamma_j$ can be obtained for any set of boundary point velocities, $\vec{U}_{\infty k}$, by matrix multiplication, which is a rather simple mathematical operation. This means that changes in angle of attack and yaw and any NUFF can be readily accommodated without repeating the relatively complex operation of matrix inversion.

Once the vortex strengths, $\Gamma_j$, are obtained for a specific set of boundary point velocities, the velocity field is obtainable from Eq. (15) and the pressure coefficient at any point (except on the body surface) is given by

$$C_{p_k} = 1 - \frac{|\vec{V}_k|^2}{|\vec{U}_\infty|^2}$$

### 3.4 SPECIAL CONDITIONS ON SURFACE OF BODY

The concentrated vortex approximation of the surface vortex sheet provides a very good approximation of the velocity field except in the immediate vicinity of that section of the sheet approximated by a given concentrated vortex filament. In Fig. 5 it is shown that in going from the vortex sheet to the concentrated vortex approximation of a given amount of vorticity, the tangential component of the induced velocity on the vortex sheet surface attributable to that vorticity is lost. (The normal component remains the same, however, so that the application of the boundary condition at a boundary point on the surface, which is in terms of the normal velocity component only, is correct.) Therefore, to obtain the correct value of flow velocity at any point on the surface of the body, the tangential component of induced velocity attributable to the adjacent (concentrated) vorticity must be restored and added to the velocity given by Eq. (15). The magnitude of this tangential velocity increment is expressed in terms of the vorticity density, $d\Gamma/d\ell$, as

$$|\Delta\vec{V}| = \frac{1}{2}\frac{d\Gamma}{d\ell} \tag{22}$$

and $\Delta\vec{V}$ is tangential to the surface of the sheet and normal to the direction of vorticity. The vorticity density is approximated as $\Gamma/\ell$ where $\Gamma$ is the net concentrated vorticity on the segment in question, and $\ell$ is the distance over which it is compressed from distributed to concentrated vorticity. The pressure coefficient just above (zero-thickness planform) or just outside (closed surface) a boundary point is given by

$$C_p = 1 - \frac{(u + \Delta V_x)^2 + (v + \Delta V_y)^2 + (w + \Delta V_z)^2}{|\vec{U}_\infty|^2} \quad (23)$$

and similarly, just below (zero-thickness planform) or just inside (closed surface) a boundary point is given by

$$C_p = 1 - \frac{(u - \Delta V_x)^2 + (v - \Delta V_y)^2 + (w - \Delta V_z)^2}{|\vec{U}_\infty|^2} \quad (24)$$

where u, v, and w are the components of $\vec{V}_k$ and $\Delta V_x$, $\Delta V_y$, and $\Delta V_z$ are the components of $\Delta\vec{V}$.

Another situation exists on the concentrated vortex elements themselves. The distributed vorticity correction to tangential velocity is still applicable at such points, and should be made if the pressure coefficient at that point is the desired end. However, the main reason that velocities at the physical location of the vortex elements is desired is to allow calculation of force coefficients by the Kutta-Joukowski law, for which a different restriction on velocity must be observed, Section 3.5.

### 3.5 TOTAL FORCE ON BODY

There are two ways to obtain total force on a body which is approximated by a vortex-lattice network. The surface pressures obtained from Eqs. (23) and (24) can be integrated over the body surface in the conventional manner. Alternatively, the force on each elementary vortex element can be obtained by application of the Kutta-Joukowski law

$$\vec{F}_i = \rho \vec{V}_i \times \vec{\Gamma}_i \quad (25)$$

and these forces then summed. The two approaches are fundamentally equivalent and would be numerically equivalent if the solutions could be carried out in closed form. However, as a result of the numerical discreteness actually used to perform the calculations, two different approximations are possible. In the present study the latter approach was adopted, following Ref. 6.

In using the approach suggested by Eq. (25), two precautions must be observed. First, the velocity vector in Eq. (25) should not indicate any induced effects of the vortex element itself. That is, $\vec{V}_i$ should be the flow-field velocity vector which would exist in the absence of the

vortex element, but at the physical location of the element, usually assumed to be the midpoint of the element. Second, for certain cases the summation of forces given by Eq. (25) does not give the complete answer. If one returns to the exact concept of the vortex sheet, it is readily shown that Eq. (25) is equivalent to obtaining the difference in pressure load across the vortex sheet. If forces given by Eq. (25) are summed over a complete vortex network, the effect of the uniform pressure internal to a closed body cancels out, leaving only the summation of external (pressure) forces. However, when it is desired to obtain forces over only a part of the vortex network, the effect of the internal pressures does not cancel out and there will be a large unbalanced pressure force. This was found to be important in the vortex network formulation of the M-117 bomb with a trailing wake. Specifically, it was found necessary to correct the axial force determined by summing forces of the type of Eq. (25) by adding an axial-force correction equal to the bomb base area times the pressure in the imaginary flow internal to the bomb surface, essentially stagnation point pressure.

# SECTION IV
# DESCRIPTION OF COMPUTER PROGRAM DEVELOPED FOR VORTEX–LATTICE CALCULATIONS

## 4.1 BACKGROUND

The method of determining the steady, incompressible, potential flow aerodynamic characteristics of three-dimensional surfaces by representing planforms with a vortex-lattice has been incorporated in a number of different computer programs in recent years. Among the programs which have found application in industry one of the earlier efforts, performed at The Boeing Company, is described in Ref. 6. One of the most recent developments of a computational procedure has been performed at the Langley Research Center (Ref. 7) and has resulted in a program that is designed to readily accommodate planforms of particularly complex geometrical configurations. The first program cited above, Ref. 6, has been utilized in a modified form at AEDC in applications which include modeling V/STOL aircraft problems and struts and model supports (Ref. 8). Reference 8 describes a means of incorporating the effect of compressibility in the analysis using linearized, small perturbation airfoil theory.

## 4.2 DESCRIPTION

The theoretical results presented in this report were obtained from a computer program written ab initio (in the FORTRAN IV language) using the equations for vorticity, velocity, pressure coefficient, and force and moment coefficients given in Ref. 6. This new program differed from that of Ref. 6 in that more efficient influence coefficient routines were used which eliminated duplication of purely geometric calculations and, in addition, a capability for nonuniform flow boundary conditions was added. Because of the conflicting requirements of calculational efficiency and computer memory capacity in terms of the number of vortices which can be handled, two different versions of this vortex-lattice program have been developed. The simpler version (designated as Program PRP 16) is restricted to a relatively small number of vortices which, in turn, requires only brief computational times. Consequently, this program has proved to be a useful tool to develop familiarity with the vortex-lattice technique and to perform studies of the modeling requirements of various physical shapes. This program has been used for some of the simpler models representing the M-117 bomb and for investigation of some of the fine points of representation of a physical shape by concentrated vortex elements. The entire potential flow solution is obtained with a single input of punched cards, the output is written in printed format, and no magnetic tapes are required.

The accuracy of results is a sensitive function of the number of discrete elementary vortex filaments used to approximate the actual continuously distributed vorticity at the surface of the body. In order to be able to attain more accurate results than are possible with PRP 16, a second version (designated as PRP 28) of the basic program has been developed which can accommodate a greater number of vortex elements. This is accomplished by segmenting the program into three separately compiled job steps (for descriptive purposes these steps will be referenced in this report as PRP 28A, PRP 28B, and PRP 28C). Since the source program for each of these steps is stored in a smaller portion of the core than is required for PRP 16, this saving of core memory is used to store larger matrices that arise in the intermediate calculations of an increased number of vortices. Whenever a different geometric model is postulated, the potential flow calculations must be initiated from the beginning which results in lengthy execution times. However, when the computations that are purely a function of model geometry are completed (in PRP 28A and PRP 28B) and stored on magnetic tape, the subsequent calculations for vorticity, velocity, pressure coefficient, and aerodynamic force and moment coefficient distribution can be rapidly performed (in PRP 28C) for parametric variations of

(1) incidence of the body with respect to the undisturbed free stream and (2) variations in the nonuniform flow field induced by a neighboring body. Whereas the input/output media, use of intermediate memory devices, and job step arrangement are different for the two programs, the computational techniques described below are essentially the same.

## 4.3 COMPUTATIONAL TECHNIQUES

The execution of the solution begins with the specification of coordinates that define straight-sided panels approximating the actual planform (Fig. 4a). The bound vortex filaments are taken to be coincident with the edges of these panels (Fig. 4b). The coordinates are given in a store body-axis reference system in order to render the calculations of the geometric quantities invariant with respect to the spatial orientation of the body.

The criterion used in the course of this analysis for specifying fin coordinates on the M-117 bomb fins was straightforward - uniform chordwise and uniform spanwise spacing - and resulted in no numerical difficulties. On the body of the bomb a uniform spanwise (circumferential) spacing at each longitudinal station was used in all the solutions, and this gave no computational problems. In the chordwise (longitudinal) direction different spacings were used on the bomb body in the various solutions; in some instances the spacing was approximately uniform, and in other instances the spacing was varied (in an irregular manner) over the length of the body. It was found that the results can be critically dependent upon the manner in which the coordinates are specified in the chordwise direction, which is discussed in more detail in Section 5.1.2.

In order to complete the specification of the geometric factors required by the vortex-lattice method, a procedure for locating the control points at which the tangential flow boundary condition is to be satisfied must be determined. Rules for locating both the vortex networks as well as these control points (referred to as boundary points) are given in Ref. 6 where a method of representation of a surface was assumed to be optimum when the forces and vorticity distribution were found to be independent of the number of vortices used to represent the surface, and were of a magnitude corresponding to that predicted by other theories and experiment. The criterion for boundary point location used in obtaining the results described in this report combines simplicity and plausibility - the boundary point coordinates are taken to be the arithmetic average of the end points of the surrounding vortex

segments. This criterion for locating boundary points appeared to be satisfactory, judging by the results of the solutions, with one notable exception, which is discussed in Section 5.1.2.

Subsequent to the calculation of the matrices containing only geometric quantities (G and H, defined by Eqs. (14) and (18)), the inversion of the H matrix is performed. Two different algorithms are used to effect the inversion, depending upon whether or not the flow field is symmetric about the x-z plane (a yawing attitude or a NUFF with sidewash components will produce asymmetry). The explanation for this is shown by writing the matrix equation for vorticity, Eq. (19), for the general nonsymmetrical case, and then noting how the equation can be simplified in the case of no yaw and free-stream boundary conditions symmetric about the x-z plane of symmetry. Let Eq. (19) be written in the partitioned form

$$\left[\begin{array}{c|c} H^{(1)} & H^{(2)} \\ \hline H^{(2)} & H^{(1)} \end{array}\right]\left\{\begin{array}{c} \Gamma^{(1)} \\ \hline \Gamma^{(2)} \end{array}\right\} = \left\{\begin{array}{c} C^{(1)} \\ \hline C^{(2)} \end{array}\right\} \tag{26}$$

where $H^{(1)}$ contains the influence of vortices on the +y side of the x-z symmetry plane at control points on the +y side; $H^{(2)}$ contains the influence from the -y side on the +y side; $\Gamma^{(1)}$ is the vector of strengths of vortices on the +y side, and $\Gamma^{(2)}$ is the vector of vortex strengths on the -y side. Terms $C^{(1)}$ and $C^{(2)}$ are the components of free-stream velocity normal to the surface (normalized by $H_{k,k}$, the elements of the principal diagonal of the matrix defined by Eq. (18)) on the ±y sides of the x-z symmetry plane, that is, $C_k^{(\ell)} = -(\vec{n} \cdot \vec{U}_\infty)_k^{(\ell)}/H_{k,k}$, $\ell = 1, 2$. The significance of a zero yaw attitude combined with symmetry of free-stream flow field is that fulfillment of these two conditions implies the vorticity distribution is symmetric about the x-z plane, that is, $\Gamma^{(1)} = -\Gamma^{(2)}$. The matrix equation for such a case thus reduces to

$$\left\{\Gamma^{(1)}\right\} = \left[H^{(1)} - H^{(2)}\right]^{-1}\left\{C^{(1)}\right\} \tag{27}$$

In the more general case of asymmetry about the x-z plane the inversion of Eq. (26) is obtained using

$$\left\{\begin{array}{c} \Gamma^{(1)} \\ \hline \Gamma^{(2)} \end{array}\right\} = \left[\begin{array}{c|c} A^{(1)} & A^{(2)} \\ \hline A^{(2)} & A^{(1)} \end{array}\right]\left\{\begin{array}{c} C^{(1)} \\ \hline C^{(2)} \end{array}\right\} \tag{28}$$

where

$$A^{(1)} \equiv \left[ I - H^{(1)^{-1}} H^{(2)} H^{(1)^{-1}} H^{(2)} \right]^{-1} H^{(1)^{-1}}$$

$$A^{(2)} \equiv \left[ I - H^{(1)^{-1}} H^{(2)} H^{(1)^{-1}} H^{(2)} \right]^{-1} \left[ - H^{(1)^{-1}} H^{(2)} H^{(1)^{-1}} \right]$$

In deriving Eq. (26) the elements of the H matrix (given by Eq. (18)) have been normalized so that all elements on the principal diagonal of $H^{(1)}$ have the value unity in order to enhance the conditioning of H with respect to inversion. The inversions are performed using the Gauss-Jordan method of complete pivotal condensation. As an optional diagnostic feature, the results are checked by forming the product $H^{-1}H$ and comparing this with the identity matrix. A further check on the solution is obtained by computing the product $H\Gamma$ and comparing this with the C matrix.

The remaining calculational techniques involve a straightforward implementation of formulas given in Ref. 6, with the exception of the specification of the free-stream flow field in which the body being analyzed is immersed. The free-stream velocity is characterized by a spatially varying (x, y, and z directions) NUFF distribution prescribed at a finite set of points comprising a control volume about the body. (A program option is available which permits specification of a uniform free-stream velocity vector.) The values of free-stream velocity which are used in the computations are required at points on the panels approximating the planform geometry. In general, these points have different spatial locations than those at which the NUFF values are input to the programs. The values used in the calculations are obtained from a three-dimensional interpolation of the input NUFF values. The computer programs, as presently coded, have no provision for free-stream sidewash and also require the magnitude (but not the direction) of the free-stream velocity vector to be uniform throughout the flow field. The removal of these two restrictions would require only a small effort.

## 4.4 COMPUTER PROGRAM CAPABILITIES

The capabilities of the computer program developed during the course of this analysis will be described with regard to modeling, maximum number of vortices and selection of variables to be computed.

### 4.4.1 Modeling Capabilities

Programs PRP 16 and 28 have been written so that analyses may be performed for geometrical configurations of a very general nature. A configuration is composed of an arbitrary number of components. In order to facilitate the subsequent discussion, the terminology of Ref. 6 is employed in which these components are referred to as "wing parts."

When two or more wing parts are adjacent to each other such that vortex segments on one wing part coincide with vortex segments on the other, special treatment is required in the calculation of forces along these segments, and also in the computation of pressure coefficients at the boundary points adjacent to the common vortex segments. As regards the evaluation of forces along these segments, this is purely a coding detail and not a physical problem since the net force increment along such a junction is the superposition of the contributions from the individual wing parts. When the general formula for pressure coefficient, Eqs. (23) and (24), is applied at boundary points adjacent to a junction line of wing parts assumptions of a physical nature as well as coding details are involved. The necessity of invoking additional assumptions stems from the fact that the concentrated vortices comprising the vortex-lattice actually represent vorticity distributed on the surface, and the influence of this distributed vorticity on the velocity at the boundary points must be computed in solving for the pressure coefficients. The assumptions mentioned above require specifying the manner in which the vorticity that is concentrated along a line common to more than one wing part should be distributed over the adjacent wing parts. Whereas the subject programs could be modified to accommodate any desired approach to this problem, the method that has been incorporated is to distribute Vortex A over Wing Part 1, and Vortex B over Wing Part 2 in the example shown. This scheme possesses the advantage that it can be applied to combinations of planforms of arbitrary configuration without requiring any change in coding.

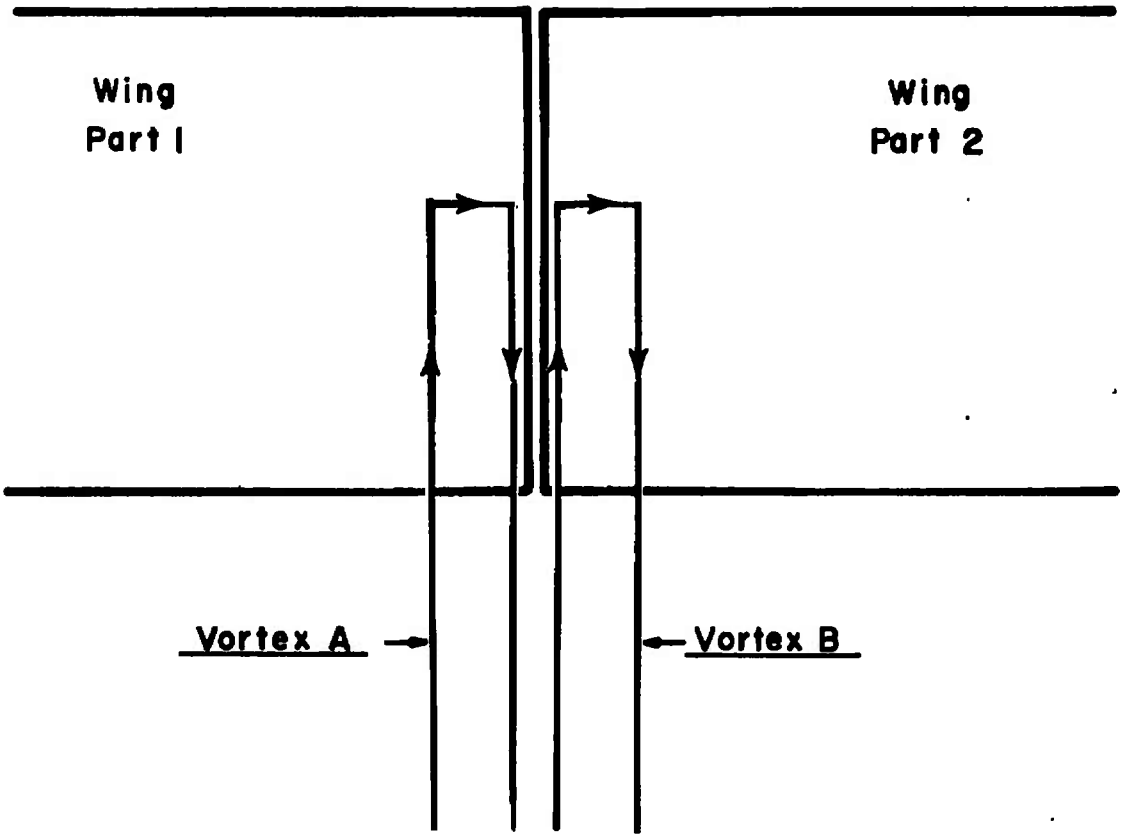


The modeling capabilities are such that the streamlines of the flow field which are attached to the body can be constrained to lie on any extension of the body, either upstream or downstream. A possible application of an upstream extension would be the simulation of only the aft portion of a thick body - the entire body presenting an intractable problem. Possible applications of downstream extensions would be to enforce a postulated wake geometry, or to impose a Kutta condition that the flow leave a zero-thickness trailing edge smoothly.

#### 4.4.2 Maximum Number of Vortices

The accuracy of the results is a function of the number of vortices used in the analysis. (Whenever reference is made hereafter to a specific number of vortices, it will indicate the number on only one side of the x-z symmetry plane.) The permissible number of vortices in both PRP 16 and PRP 28 is limited by the requirement of performing matrix inversions in the core. This in-core inversion requirement is a consequence of using an inversion algorithm that repeatedly processes all the elements of a two-dimensional array; presumably the maximum number of vortices could be increased if partial, rather than complete, pivoting were used since this would require that only one row of data

need be retained in the core memory at any given time. The permissible number of vortices are approximately

| PRP 16 | | PRP 28 | |
|---|---|---|---|
| No Yaw | With Yaw | No Yaw | With Yaw |
| 85 | $85/\sqrt{2}$ | 180 | $180/\sqrt{2}$ |

for calculation by a computer whose Central Processing Unit (CPU) can store a source program of 45,000 decimal words using internal memory. If a CPU with a larger memory unit were employed, almost all of the increased capacity could be utilized to store additional elements of the H matrix resulting from an increased number of vortices.

### 4.4.3 Optional Selection of Variables to be Computed

The computer programs which were used to produce the results reported herein can be controlled so that the variables of primary importance which are obtained in the solutions consist of any, or all, of the three following sets:

1. Horseshoe vortex strength, $\Gamma_j$, from either Eq. (27) or Eq. (28) depending upon whether or not the flow field is symmetrical about the x-z geometrical plane of symmetry; resultant velocity at the boundary points (free stream, $\vec{U}_\infty$, plus induced, $\sum_{j=1}^{N_j} \vec{q}_{k,j}$, from Eq. (13), plus distributed vorticity contribution, $\Delta\vec{V}$, using Eq. (22)); pressure coefficient, $C_p$, at the boundary points from Eqs. (23) and (24).
2. Force and moment coefficients (lift, drag, side force, pitch, roll, and yaw) resulting from the individual (linear) bound vortex segments - in addition to the corresponding coefficients for the entire body obtained by summing the appropriate segment coefficients.
3. Resultant velocities at specified points in the flow field off the surface of the body, from an expression of the form of Eq. (15).

All variables are referred to a body-axis coordinate system with the exception of the force and moment coefficients, which are given in a wind-axis reference system.

### 4.5 COMPUTING TIME

The vortex-lattice solutions reported herein were obtained on an IBM 360/50 digital computer. Examples will be cited of computational times required to execute solutions. The time required varies as the square of the number of vortices since the execution time is primarily a function of the size of the matrices containing the geometric factors and the number of elements in these matrices varies as the number of vortices squared. A representative calculation assuming 156 vortices (and symmetry of flow about the x-z plane) required one hour to compute the G, H, and $H^{-1}$ matrices and write these on magnetic tape. An additional 3 min per case was required to perform the calculations for vorticity, velocity, pressure coefficient, and force and moment coefficients (a case means one value of angle of attack). When asymmetry about the x-y plane (resulting from a yaw attitude or lateral variation of free-stream boundary conditions) is included, the time is increased by about 50 percent.

## SECTION V
## POTENTIAL FLOW OVER M-117 BOMB

### 5.1 REPRESENTATION OF BOMB BY VORTEX NETWORKS

A number of different vortex networks representing the M-117 bomb were evaluated to obtain a potential flow solution with force characteristics reasonably close to wind tunnel values.

#### 5.1.1 Successful Networks

Vortex elements were chosen as the flow singularities to be used because of the need to represent trailing vorticity in the flow due to the bomb fins. It was initially decided that there was to be no trailing vorticity from the bomb body, hence a network was assumed in which the trailing segments of horseshoe vortices were brought together and cancelled before leaving the body. The horseshoe elements were assumed to begin at the base of the bomb and "trailed" forward over the bomb surface to the nose, at which point the left and right segments of each horseshoe became superimposed and passed to infinity down the axis of the bomb. All successful models of the bomb were based on this swept-forward configuration of the vortex network.

The shape of the wind tunnel model of the M-117 bomb, Fig. 6, included a cylindrical base section to accommodate a force balance.

(The actual bomb shape tapers to a point in the region of the base.) During the development phase of the vortex-lattice computer program, the simplified network of Fig. 7a was used, composed of 40 horseshoe vortices on the body and 8 on each fin, giving a total of 56 vortices to define the bomb shape on the positive side of the x-z plane. When it was found necessary to impose a wakelike character on the flow, 8 vortices were added downstream of the base of the bomb, shown as dotted lines in Fig. 7a. Another refinement was given by increasing the fin representation to 32 vortices, for a total of 112, Fig. 7b. Finally, the most complex network used was composed of 76 vortices on the body, 16 in the wake region, and 32 on each fin, for a total of 156 vortices (on half of the bomb), Fig. 7c.

### 5.1.2 Mathematically Unacceptable Networks

The three vortex networks shown in Figs. 8a through c were found to be incompatible with a potential flow solution. These three networks were formulated in an attempt to produce a wake flow at the base of the bomb. The geometric influence coefficient matrices, G, and the H matrices appeared to be normal in all respects for these networks, but upon attempting to invert the H matrices, mathematical difficulties appeared. Gigantic values for certain elements of the inverted matrices appeared with numerical values as large as $10^5$. The largest elements in the successful inversions were of the order unity. One difficulty, occurring only in the network of Fig. 8b, was that the most forward horseshoe vortices were so located that the spanwise elements formed a degenerate ring vortex of zero radius at the nose tip. The main difficulty, however, common to all three networks, was that at the last boundary point downstream of the last vortex element, it was attempted to impose on the flow a condition which was incompatible with a closure of the flow to the axis of symmetry. Such a closure was necessitated by the inability of a finite number of vortices to represent the wake all the way to infinity. It was theorized, but not actually demonstrated, that if the last boundary condition had incorporated a finite angle of closure, the solution would have become tractable. Indeed, this is precisely the situation that prevails at the nose of the bomb in the valid networks described in the previous section.

Another type of difficulty in modeling was encountered with the network shown in Fig. 8d, in which it was attempted to selectively refine the concentrated vorticity approximation in the nose region only, by doubling the number of vortex elements in the chordwise direction in this area. Although this network produced an apparently valid inversion of the H matrix, the external pressure distribution for the solution was drastically different from accepted solutions and the internal

pressure distribution departed significantly from the usual stagnation values. This anomalous behavior disappeared when the refined longitudinal spacing was extended over the entire body. Such behavior was an apparent verification of the warning given in Ref. 6 against sharp discontinuities in the spacing of vortex elements.

## 5.2 UNIFORM FREE-STREAM FLOWS

Prior to applications in disturbance fields, considerable effort was devoted to establishing an adequate potential flow calculation for the M-117 bomb in uniform free streams.

### 5.2.1 Pressure Distribution on Bomb with No Wake

Since the program being developed was a new one, some standard of comparison was desired for evaluation purposes. To this end, a source-sink solution for the bomb body alone at 0-deg angle of attack was obtained using the program of Ref. 2. The pressure distribution for a 19-element source-sink configuration is given in Fig. 9. The first mathematically successful vortex-lattice solution using 40 elements (half-body) is also given in this figure, demonstrating sufficient agreement with the source-sink solution to justify further program development, but with sufficient differences to indicate a need for a refined model. By increasing the number of vortex elements to 76, with a longitudinal spacing identical to that of the source-sink solution, the two pressure distributions were brought into very close agreement. The small remaining differences apparently result from the fact that the vortex network is discretely distributed circumferentially, whereas the source-sink solution represents a uniform distribution of singularity in this direction.

It is noted that stagnation points (and associated high pressures) are indicated at both the nose and base of the bomb for these solutions. The large negative values of $C_p$ just forward of the base reflect high velocities as the flow turns the corner at the base.

To demonstrate the importance of the distributed vorticity correction to surface velocity, Eq. (22), a typical pressure distribution on the bomb is also given for a case in which this correction has not been made, Fig. 9.

### 5.2.2 Force Coefficients on Bomb with No Wake

In Fig. 10 is given a comparison of lift and pitching-moment coefficients obtained for several vortex networks used in defining the bomb.

The case of the body alone obviously represents the D'Alembert Paradox, that is, essentially zero force, but with a finite pitching moment. The addition of the fins introduces a net lift force and simultaneously stabilizes the configuration (negative $dC_m/d\alpha$). However, the magnitude of the lift coefficient is considerably less than measured in a previous wind tunnel test as shown. Examination of the distribution of lift along the length of the bomb, Fig. 11, demonstrated that the lift developed on the nose of the bomb was offset by a negative lift contribution in the base region of the bomb, basically because of the high pressures associated with the rear stagnation point. It was apparent that better agreement with wind tunnel measurements could be obtained by imposing a wakelike flow at the base of the bomb to eliminate the negative lift contribution.

### 5.2.3 Flow over M-117 Bomb with Wake

Several attempts to construct a vortex network which would impose such a wake were unsuccessful, Section 5.1.2. Success was finally achieved by adding eight forward-running horseshoe vortices downstream of the body with corresponding boundary conditions constraining the flow to leave the base of the bomb without change of direction from the axial direction, Fig. 11. This model did allow formation of a rear stagnation point, located downstream of the last vortex element, so that in the region of the physical base of the bomb the flow was a close approximation to a wake flow. This appears in the pressure distribution curves of Fig. 12, for flows over the bomb body with and without the wake vortices. The forces on the bomb with the wake imposed were obtained by summing forces on only those vortex segments which corresponded to the physical bomb. Returning to Fig. 10, it is apparent that the addition of the wake did, in fact, result in lift and pitching moment for the complete bomb which were in reasonable agreement with the wind tunnel values.

### 5.2.4 Comparison of Optimum Vortex-Lattice Calculation with Wind Tunnel Data - Skin Friction and Base Drag Correction

Once the necessity of a wake was demonstrated on the 64-vortex model, final evaluation of the potential flow solution was performed with more complex models: the 112- and 156-vortex models of Figs. 7b and c. Since the 64-vortex model yielded $C_L$ and $C_m$ values in reasonable agreement with measurements, it was deemed reasonable at this stage to include the drag coefficient in the comparison.

The artifice of obtaining the bomb forces by summing over only a part of the vortex network – namely, those elements corresponding to the physical bomb – resulted in drag coefficients which were incorrect. In fact, fairly large values of thrust, rather than drag, were calculated. This was a result of the fact that summation of forces of the type $\rho\vec{V}_i \times \vec{\Gamma}_i$, Eq. (25), for each element of concentrated vorticity is equivalent to taking the difference in pressure load across the corresponding section of equivalent vortex sheet. Thus, the force summation corresponds to an integration of external and internal pressure loads, and if the vortex network is truncated, the integration does not cover a closed body. In the present case, the base area of the bomb body is neglected and the large internal pressure load (essentially stagnation pressure) on the base, in being omitted, results in a large axial thrust on the bomb. To correct for this omission, the axial-force coefficient must be modified by an allowance for the internal and external pressures on the base

$$C_A = (C_A)_{calc} + \frac{S_{base}}{S_{ref}} \left[C_{p_i} - C_{p_b}\right]$$

Since the present purpose is to obtain a comparison with wind tunnel measurements, it is appropriate to refer the axial force to the standard zero base drag condition ($C_{p_b} = 0$) and to make an allowance for skin-friction force

$$C_A = (C_A)_{calc} + \frac{S_{base}}{S_{ref}} C_{p_i} + \frac{S_{wet}}{S_{ref}} (C_D)_{fric}$$

where $(C_D)_{fric}$ is a flat plate skin-friction drag coefficient. The wind tunnel data were obtained at a Reynolds number of $1.1 \times 10^6$, based on the length of the bomb; consequently both laminar and turbulent skin-friction allowances were made. The comparison of calculated results and the wind tunnel measurements is given in Fig. 13 for both the 112- and 156-vortex networks. Since there is a slight dependence of $C_L$ upon $C_A$ in the usual transformation from body to wind axes, the two skin-friction allowances result in two lift curves for each model, as well as two drag curves. The pitching-moment curve, of course, is not affected. The experimental force coefficients have been (approximately) adjusted to the zero base drag condition by assuming a $C_{p_b}$ equal to the potential flow value on the base cylinder of the bomb.

A comparison of results for the two networks is as follows:

| Coefficient | Percentage of Difference between Theoretical and Experimental Coefficients: 112-Vortex Model | 156-Vortex Model |
|---|---|---|
| $C_L$, $\alpha$ = 10 deg | -17.6 | -9.8 |
| $C_m$, $\alpha$ = 10 deg | -15.0 | -5.8 |
| $C_D$, $\alpha$ = 0 deg | +200.0 | (Experimental $C_D$ between laminar and turbulent predictions) |

As should be expected, the 156-vortex solution is better in all respects. The lift and pitching-moment coefficients are within 10 percent of wind tunnel values. At small angles of attack, the theoretical values of drag (adjusted to zero base drag) are less than the measured values when a laminar skin-friction correction is made and greater when a turbulent skin-friction correction is made. This is a reasonable result for the Reynolds number of the wind tunnel test. In lieu of a more accurate calculation of location of boundary-layer transition, the laminar correction was adopted as the standard correction for skin friction.

The wind tunnel data were obtained at M = 0.49, whereas the potential flow solutions were for M = 0. Compressibility effects would reduce even further the difference between the calculated and wind tunnel data. No attempt was made to apply the usual subsonic compressibility corrections because the thickness ratio of the M-117 bomb (0.182) is large enough to place the applicability of these corrections in question. Instead, it was felt that future work would incorporate compressibility corrections from experimental data. Furthermore, it was also recognized that the ultimate use of the potential flow calculation would probably be only to give incremental corrections to force coefficients caused by flow nonuniformities. This would not necessarily require extremely high accuracy of the absolute values of force coefficients.

## 5.3 EFFECT OF NONUNIFORM FLOW FIELDS ON BOMB FORCE COEFFICIENTS

Subsequent to selection of the 156-vortex representation of the M-117 bomb for further study, the program option which accommodates nonuniform flow fields was exercised. Only the downwash angle of the free stream was allowed to vary, not the sidewash angle or magnitude of the velocity vector.

### 5.3.1 Idealized Nonuniformities

To demonstrate the NUFF capability of the program and to determine the typical magnitude of effects which physically realistic flow disturbances can produce, a set of four idealized NUFF was initially studied. These fields were formulated in simple analytic form to facilitate calculations and are shown in Fig. 14.

Case I - A constant 2.5-deg downwash throughout the field.

Case II - A linear variation of downwash in the longitudinal direction; from 2.5 deg at the nose to -1.0 deg (upwash) at the base. No vertical variation.

Case III - No longitudinal variation, but a cubic vertical variation from 2.5 deg downwash at the bomb center of gravity to 0 deg at a point 5 in. below the bomb center of gravity.

Case IV - Linear longitudinal variation, and cubic vertical variation, which is a combination of Cases II and III.

The potential flow was computed for the M-117 bomb pitched about the center of gravity in these NUFF.

An elementary consideration of simple downwash fields suggests the following possible effects:

a. A uniform downwash, $\theta_D$, should produce a simple parallel displacement of the $C_L$ and $C_m$ curves by an amount nearly equal to the downwash.

b. A longitudinal variation of downwash along the bomb should also result in a parallel shift of the $C_L$ and $C_m$ curves. The incremental effects of a longitudinal $\theta_D$ variation about a mean $\bar{\theta}_D$ should be offsetting in the local $C_L$ on either side of the location of $\bar{\theta}_D$, and additive on $C_m$, suggesting larger shifts in $C_m$ than in $C_L$.

c. A vertical variation of downwash, on the other hand, should produce changes in slope of the $C_L$ and $C_m$ curves, attributable to a variation of local downwash angle with angle of attack of the bomb. For the same reason as in (b), the effect on $C_m$ should be larger than on $C_L$, except for the special case in which $\theta_D$ reverses sign somewhere along the length of the bomb. In this

case, the incremental effects on $C_L$ and $C_m$ are reversed and the larger effect would be expected in the $C_L$ curve. However, in this special case $\bar{\theta}_D$ is also small, so that expected effects on both $C_L$ and $C_m$ are small.

The results of the calculation of force and moment coefficients for the four simple NUFF are given in Fig. 15. Several points of agreement with the simple predictions just listed are apparent. The $C_L$ and $C_m$ curves for Case I are clearly shifted by 2.5 deg along their entire length, in agreement with (a). The Case II curves appear to demonstrate (b) above, except for the direction of displacement. Since the $\bar{\theta}_D$ for this case is +0.75 deg, yet the $C_L$ and $C_m$ curves are displaced -1.0 and -2.5 deg, respectively, it appears that the base of the bomb is affected disproportionately more by the nonuniformity than is the nose. The curves of Case III distinctly exhibit the changes in slope predicted in (c), including the greater change in slope for the $C_m$ curve. Although Case IV possesses a vertical variation of downwash which would, in most cases, produce changes in slope of the $C_L$ and $C_m$ curves, it is an example of the special case cited in (c) in which $\theta_D$ reverses sign and yields only very small changes in slope.

The changes in drag coefficient produced by the four NUFF appear to be larger than one would expect from a simple consideration of small variations of downwash. Horizontal shifts of the $C_D$ curves parallel to the $\alpha$ axis would be expected, with relatively minor changes in minimum drag coefficient. In Fig. 15, the $C_{D_o}$ can be seen to change by up to 50 percent for Case III. Although the fundamental reason for the unexpectedly large effects of the NUFF is not known, it is noted that these effects are not inconsistent with the variations of the experimental drag coefficients, Section 5.3.2.2.

A summary of the effects of the four NUFF on the three force coefficients is as follows, where the values in the table are the changes with respect to the uniform flow values:

| | $C_L$ | | $C_m$ | | |
|---|---|---|---|---|---|
| Case | $\Delta\alpha_o$, deg | $\Delta$Slope, percent | $\Delta\alpha_o$, deg | $\Delta$Slope, percent | $C_{D_o}$, percent |
| I | 2.5 | 0 | 2.5 | 0 | -4 |
| II | -1.0 | -2 | -2.5 | -3 | 18 |
| III | 2.5 | 6 | 2.3 | 11 | 52 |
| IV | -1.0 | -3 | -2.6 | -5 | 20 |

### 5.3.2 F-4C Experimental Downwash Field

The potential flow calculations were next extended to a more realistic NUFF, namely that existing beneath the F-4C aircraft. Unfortunately, expiration of the project allowed only a preliminary application of this flow field in a rather approximate manner. The parent aircraft configuration is shown in Fig. 16. It includes the basic F-4C, a 370-gal fuel tank on the outboard pylon, and an empty triple ejection rack (TER) on the inboard pylon. This configuration was chosen as the parent configuration because it was the only one for which both flow-field measurements and bomb force measurements at various locations within the field were available. The distribution of downwash angles in the F-4C flow field at M = 0.49 with the parent aircraft pitched to a 0.3-deg angle of attack is presented in Fig. 17. (The complete flow velocity vector was measured during the wind tunnel tests using a five-orifice conical flow angularity probe; however, only the downwash data are presented here.)

#### 5.3.2.1 Effect of F-4C Flow Field on Bomb Forces - Potential Flow Calculation

By a minor addition to the potential flow program developed for this project, the capability of complete allowance for NUFF as boundary conditions on a store in the simple interference regime could be obtained. Because of time limitations, actual application was restricted to the approximate case of zero sidewash components and a downwash field which varied in the X- and Z-directions but which was constant in the Y-direction. Calculation of store forces in this approximation was a preliminary step but can be considered of importance for purposes of demonstration of the program capability.

The potential flow results for three vertical positions of the bomb directly beneath the carriage position on the TER, X = 12.99 in., are given in Fig. 18 as $C_L$, $C_m$, and $C_D$ versus angle of attack. The bomb was pitched about the nose rather than the center of gravity in this case because the wind tunnel test was conducted in this manner. There can be seen a generally consistent trend of the force coefficients towards the uniform flow values as the bomb is positioned farther and farther away from the aircraft, as would be expected from the downwash curves of Fig. 17. The size of the incremental effects of the F-4C NUFF on the force coefficients is less than for the idealized case of Fig. 15 because the downwash angles encountered are smaller. From Fig. 17 it is observed that at Y = 4.66 in. the average downwash over the length of the bomb is approximately +0.75 deg, whereas all the $\Delta\alpha_o$'s in Fig. 18 are negative, except for the $C_L$ curve at Z = 7.13 in. The appearance of

negative $\Delta\alpha_o$ for positive $\bar{\theta}_D$ indicates a predominance of the fins and base of the bomb over the nose of the bomb in determination of the effects of the NUFF. A maximum incremental change in the slope of the $C_m$ curve (referred to the uniform flow case) is -2.5 percent at Z = 5.13 in., for which case the change in the $C_L$ curve is -1.4 percent. The effect of the disturbance field on the drag coefficient is an increase in $C_D$ at locations closest to the aircraft, amounting to 16.5 percent increase at Z = 3.13 in.

The potential flow results for a series of four horizontal locations of the bomb at a constant vertical distance (Z = 3.13 in.) below the F-4C are given in Fig. 19. Here, again, a very regular variation of force coefficients with position is observed, although the asymptotic approach to uniform flow values does not occur because the most forward position of the bomb is clearly still in the disturbance region. The $\Delta\alpha_o$'s vary from -0.4 to 0.6 deg for $C_L$ and from -0.2 to -1.0 deg for $C_m$. The maximum slope change is 1.1 percent for $C_m$ and 1.4 percent for $C_L$. The minimum drag coefficient varies regularly from an 8.5-percent increase to a 23-percent increase over the uniform flow values.

From Figs. 18 and 19, the general effects of the F-4C NUFF may be summarized. As the bomb is moved vertically towards the aircraft at a longitudinal position corresponding to the carriage position, $C_L$ increases, $C_m$ decreases, and $C_D$ increases. As the bomb is moved towards the aircraft from the upstream direction, at a vertical position 2.5 bomb diameters beneath the aircraft, $C_L$ increases, $C_m$ decreases, and $C_D$ decreases.

#### 5.3.2.2 Effect of F-4C Flow Field on Bomb Forces - Experimental Measurement and Comparison with Potential Flow Calculation

Although the potential flow calculations did not correspond to a proper application of the experimental F-4C flow field as boundary conditions (because of the limitations of zero sidewash and a two-dimensional downwash field), a comparison with experimentally measured force coefficients is nevertheless of interest to determine if at least the proper trends are followed.

The experimental force coefficients are given in Fig. 20 for the same positions of the bomb as in the vertical series of Fig. 18. The agreement of calculated and measured force coefficients in terms of absolute magnitude is no better than that observed in the case of uniform flow, Fig. 13. But, it is not the absolute magnitudes which are

of primary concern. A method of force prediction (leading to store separation prediction) has been proposed which would rely on calculated incremental effects of a given NUFF for correction of store force coefficients measured in a uniform flow.

If the incremental effects of the NUFF on the bomb force coefficients are next considered, both favorable and unfavorable results can be observed. The unfavorable result is represented by opposite signs of the $\Delta\alpha_o$ in the calculated and experimental data. That is, considering incremental effects with respect to uniform flow values, there is no agreement between experiment and theory. A favorable result is found in the observation that the $C_L$ and $C_m$ curves for the various values of Z are distributed in the same order in theory and experiment, independent of the relation to the uniform flow curves. This implies that the incremental effects obtained within the NUFF itself (ignoring the uniform flow values) are in agreement. This can be observed more clearly in Fig. 21, in which $C_L$ and $C_m$ are given as functions of Z for both calculated and experimental data, at constant values of $\alpha$ from -4 to 6 deg. If one considers only $3.13 \leq Z \leq 7.13$, thus ignoring the uniform flow values, the incremental effects of the NUFF are remarkably similar in shape for theory and experiment. The similarity is more pronounced in the $C_L$ curves than in the $C_m$ curves, but is remarkable in either case when one considers the approximate manner in which the NUFF boundary conditions were applied in the calculation. Better agreement yet would be expected upon proper application of the boundary conditions. Even in the present approximation, a fair prediction of the experimental force coefficients in the range of Z from 3 to 7 in. could be made, using only the measured values at Z = 7.13 in. and the incremental corrections obtained from the potential flow solutions. This must be considered as fairly convincing evidence of the ultimate possibility of using potential flow solutions to modify uniform flow store force coefficients in store separation predictions.

The incremental effects on drag coefficient, even in the range of Z = 3.13 to 7.13, are much larger in the experimental measurements than in the theoretical calculations, although the direction of change is the same in each case. This may be a result of changing base drag, which is not allowed for in the potential flow calculation. In any case, the bomb drag is not an important parameter in store separation.

The situation with regard to the uniform flow force coefficients can be further considered. In Fig. 21, for Z > 7.13 in., it is apparent that neither the experimental nor the calculated $C_L$ and $C_m$ curves fair smoothly to the uniform flow result in an asymptotic manner, as should be the case. The potential flow curves come close to such behavior,

however, indicating some small, unaccounted effect in the calculations. In the case of the experimental curves, however, the apparent disagreement between $C_L$ and $C_m$ and the uniform flow values at the maximum value of Z at which they were measured is so large that one or the other is apparently in error.

## SECTION VI
## RESULTS

1. Consideration of the requirements of analytical store separation prediction suggested the most important element of such analysis would be an accurate calculation of forces on a store when located in the disturbed flow field produced by a parent aircraft.
2. Two computer programs were developed for calculation of exact potential flows over vortex networks representing typical stores at M = 0. The lift and pitching-moment coefficients calculated for the M-117 bomb represented by 156 horseshoe vortices were found to agree with wind tunnel measurements at M = 0.49 to within 10 percent. For small angles of attack, the calculated drag coefficient (adjusted to zero base drag) was less than experimental when a laminar skin-friction correction was made and greater than experimental when a turbulent skin-friction correction was made.
3. A provision was made, valid in the simple interference regime, for the imposition of nonuniform flow boundary conditions. Flows were calculated for the bomb immersed in both idealized nonuniformities and in the actual disturbance field measured beneath the F-4C aircraft. In each case, only the downwash component of nonuniformity was considered.
4. In the idealized nonuniform flows the calculated force coefficients agreed with qualitative predictions and demonstrated in most cases the greater effect of nonuniformity on pitching moment than on lift.
5. In the F-4C flow field the calculated force coefficients were observed to display very nearly the same incremental behavior as did experimental force coefficients, even though the application of nonuniform boundary conditions was incomplete. This equivalence of incremental

behavior suggests the possibility of obtaining accurate force coefficients in disturbed flow by simply adding theoretical corrections to values measured with good accuracy in uniform flow.

6. Optimization of the vortex network was based on comparison with wind tunnel measurements and with pressure distribution on the bomb body calculated by a source-sink method. The usual dependence of accuracy on number of vortices was observed with the final optimum configuration utilizing 156 vortices to represent half of the M-117 bomb. An equally important factor was found to be elimination of the rear stagnation point by adding more vortices to impose a wake flow at the base of the bomb. In the process of optimizing the vortex network, a number of empirical rules for avoiding mathematically unacceptable networks were formulated.

7. For an IBM 360/50 digital computer having an internal memory of 45,000 decimal words, a single potential flow calculation for the M-117 bomb using 156 vortices was found to require one hour of computer operation. However, once the initial geometric part of the solution was obtained, subsequent solutions for any other set of boundary conditions, that is, angles of pitch or yaw or any nonuniform flow field, could be obtained in three minutes of computer operation.

## REFERENCES

1. Grose, Gordon G., and Woodward, Frank A. "Evaluation of the Prediction of Airplane/Store Interference by Linear Theory." Aircraft/Stores Compatibility Symposium Proceedings, Armament Development and Test Center, Eglin Air Force Base, Florida, Vol. V, November 19-21, 1969, pp. 5-79 to 5-112.

2. Smith, A. M. O. and Pierce, Jesse. "Exact Solution of the Neumann Problem. Calculation of Non-Circulatory Plane and Axially Symmetric Flows about or within Arbitrary Boundaries." Douglas Company, El Segundo Division, Report ES 26988, April 1958.

3. Rubbert, P. E., Saaris, G. R., Scholey, N. B., Standen, N. M., and Wallace, R. E. "A General Method for Determining the Aerodynamic Characteristics of Fan-in-Wing Configurations. Vol. I - Theory and Application." U. S. Army, USAAVLABS Tech. Rep. 67-61A, December 1967.

4. Durand, W. F. Aerodynamic Theory. Vol. I, pp. 386-387, and Vol. II, pp. 14-17, Dover, New York, 1963.

5. Brand, Louis. Vector Analysis. Wiley, New York, 1957.

6. Rubbert, Paul E. "Theoretical Characteristics of Arbitrary Wings by a Non-Planar Vortex Lattice Method." Boeing Company, Document No. D6-9244, February 1964.

7. Margason, R. J. and Lamar, J. E. "Vortex-Lattice FORTRAN Program for Estimating Subsonic Aerodynamic Characteristics of Complex Planforms." NASA TN D-6142, February 1971.

8. Robson, G. D. "A Method for Computing Flow Angularity and Mach Number Deviation in Subsonic Compressible Flow as Induced by Struts and Model Supports." Unpublished Master of Science Thesis, The University of Tennessee, Knoxville, Tennessee, August 1967.

# APPENDIX
# ILLUSTRATIONS

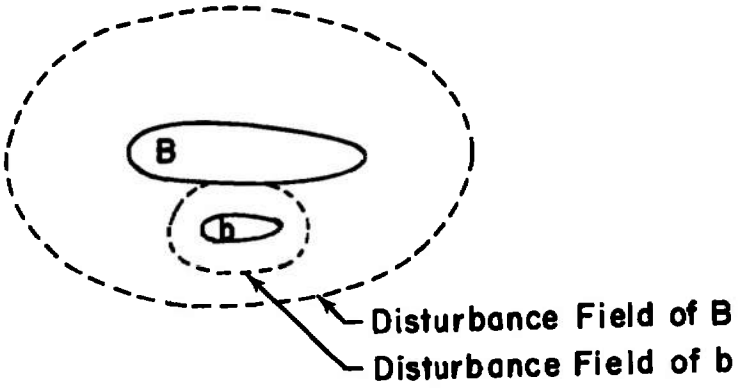


a. Mutual Interference Regime, $B \overset{Int.}{\leftrightarrow} b$

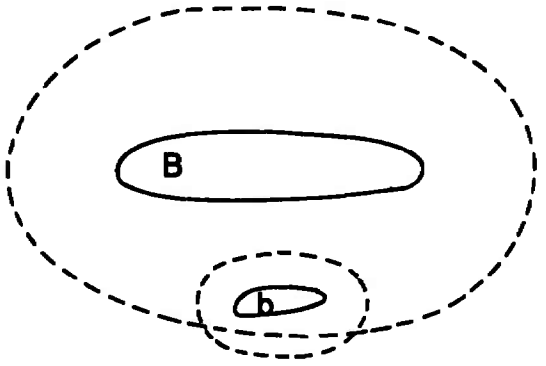


b. Simple Interference Regime, $B \overset{Int.}{\rightarrow} b$

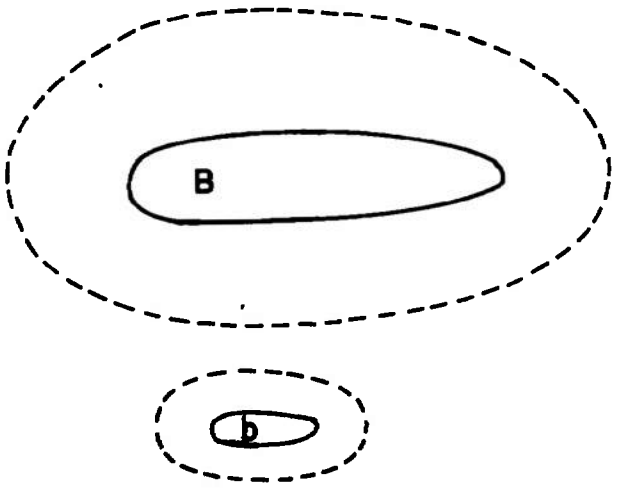


c. No Aerodynamic Interference

Fig. 1 Two-Body Flow-Field Interference

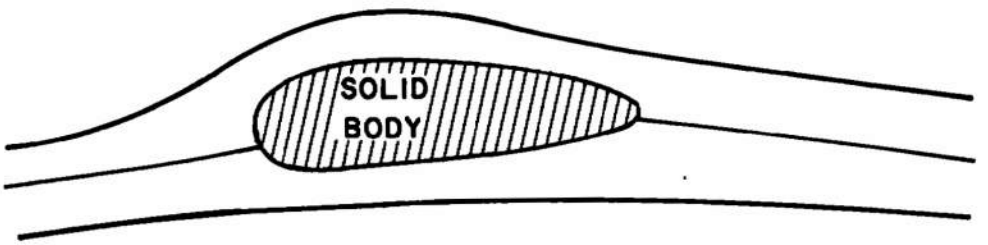


a. Solid Body Immersed in Fluid Flow

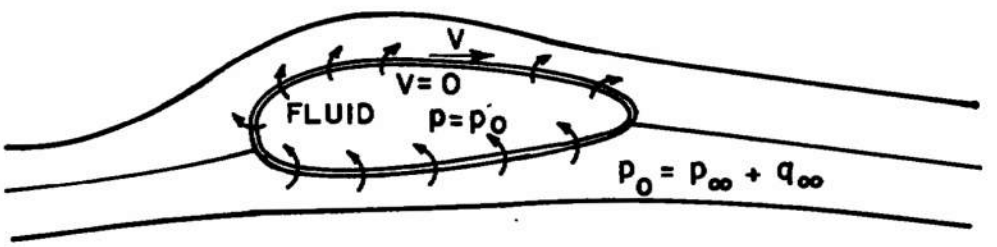


b. Solid Body Replaced by Fluid at Rest, Boundary Surface Becomes a Vortex Sheet

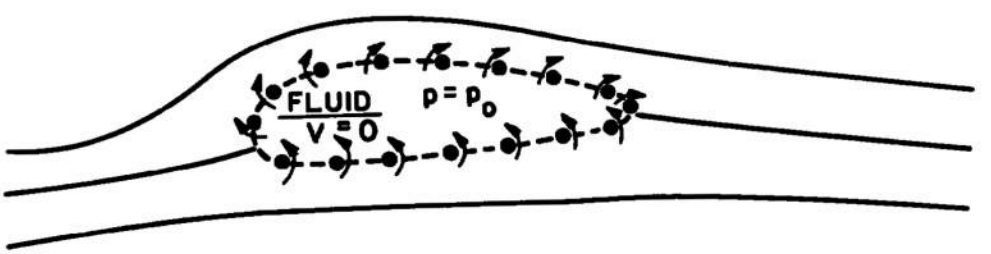


c. Vortex Sheet Approximated by Concentrated Vortex Filaments Distributed on Surface

Fig. 2 Vortex Representation of a Solid Body

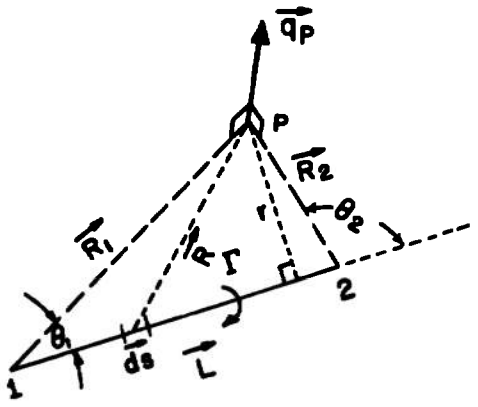


Fig. 3 Vector Relationships of Biot-Savart Law

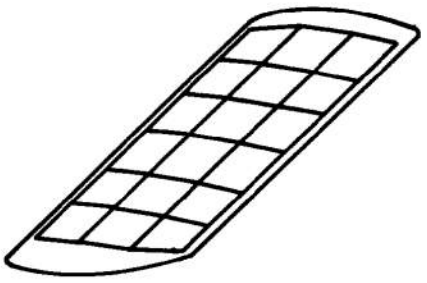

a. Quadilateral Vortex Panels

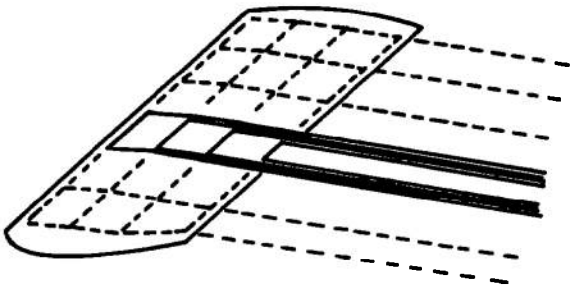

b. Horseshoe Vortex Network

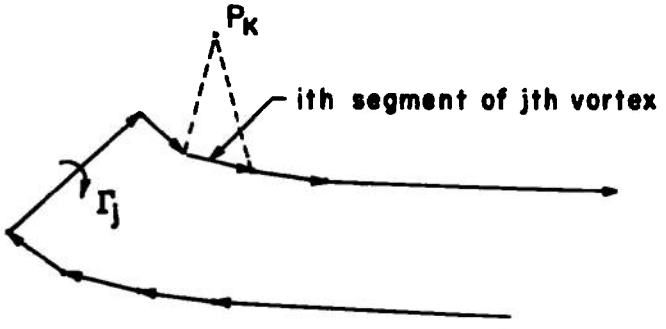


c. Single Horseshoe Vortex

Fig. 4 Surface Representation by Vortex Networks

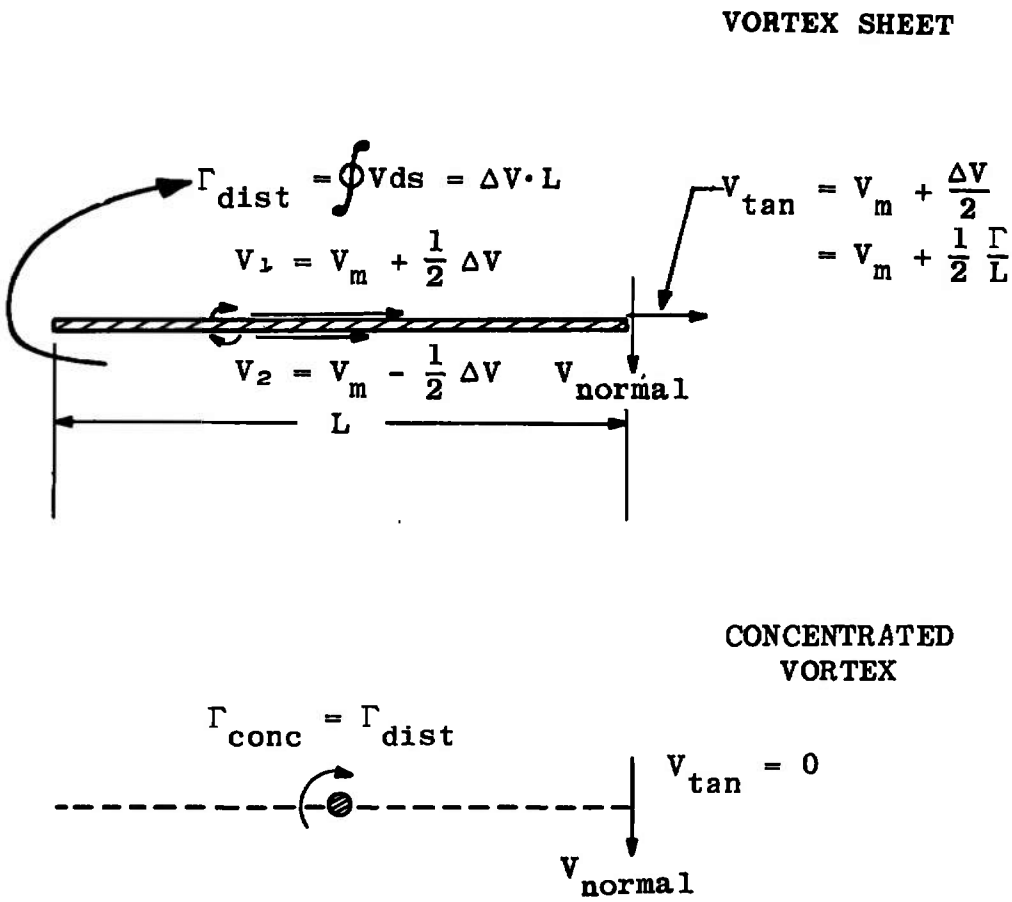


Fig. 5 Approximation of Vortex Sheet by Concentrated Vorticity

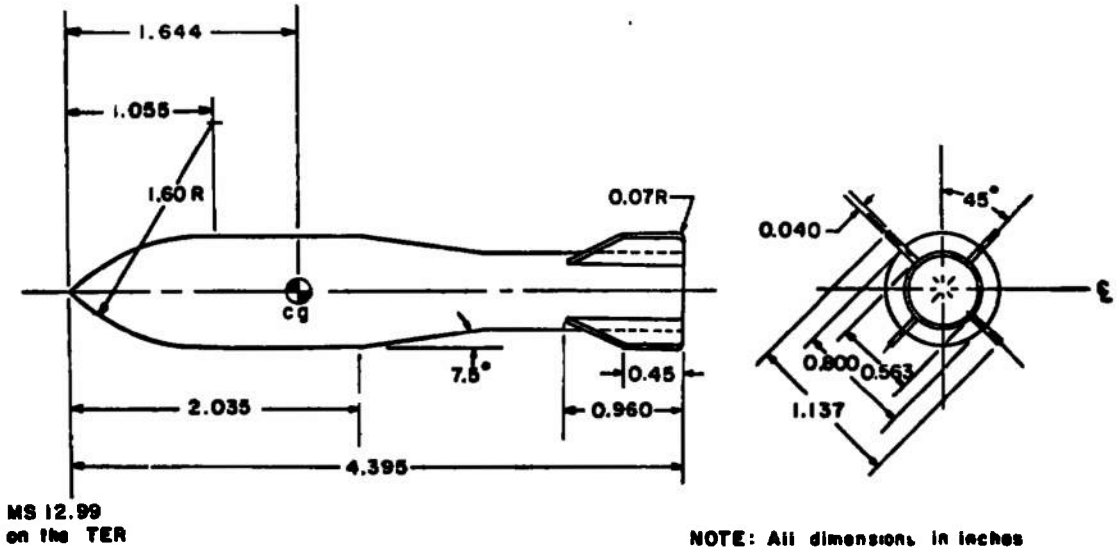


Fig. 6 Dimensional Sketch of 1/20-Scale M-117 Bomb Model

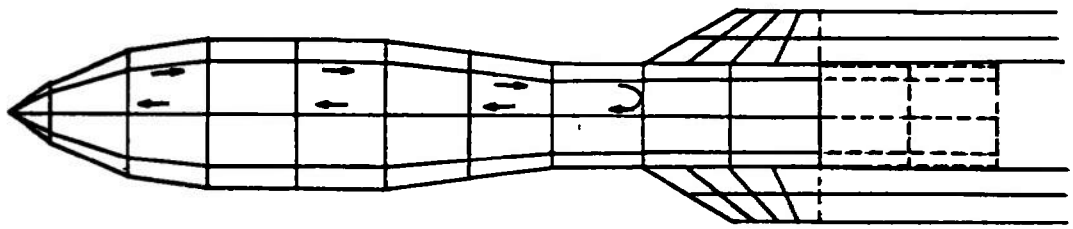

a. 64-Vortex Model

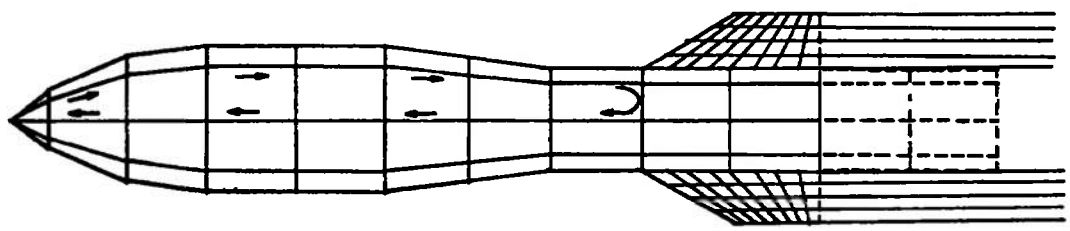

b. 112-Vortex Model

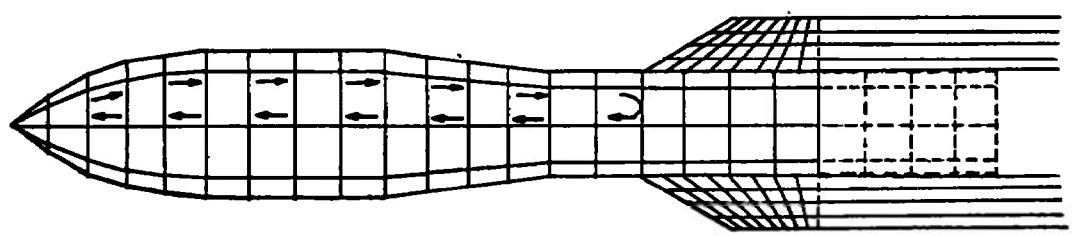

c. 156-Vortex Model

Fig. 7 Successful Vortex Networks for Approximation of M-117 Bomb

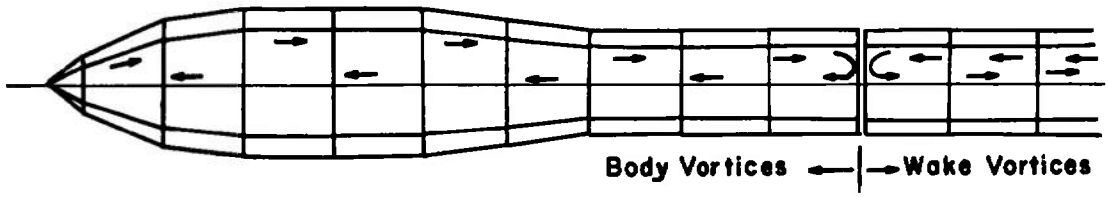


a. Body Vortices Swept Upstream, Wake Vortices Swept Downstream

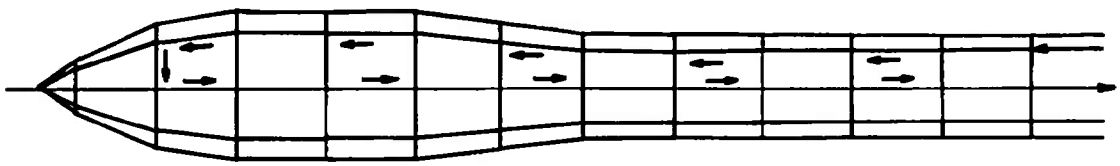

b. Body and Wake Vortices Swept Downstream, Sharp Nose

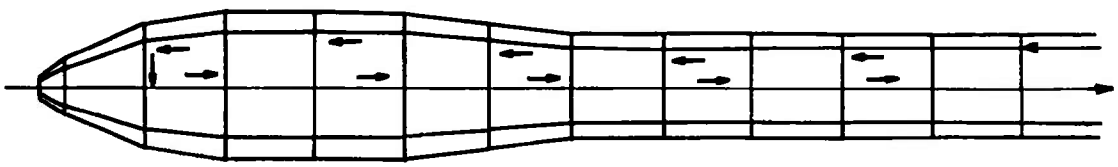

c. Body and Wake Vortices Swept Downstream, Blunted Nose Tip

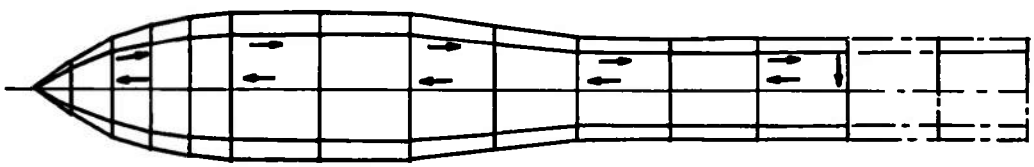

d. Body and Wake Vortices Swept Upstream, Reduced Spacing of Vortices on Nose Only

Fig. 8 Unsuccessful Vortex Networks

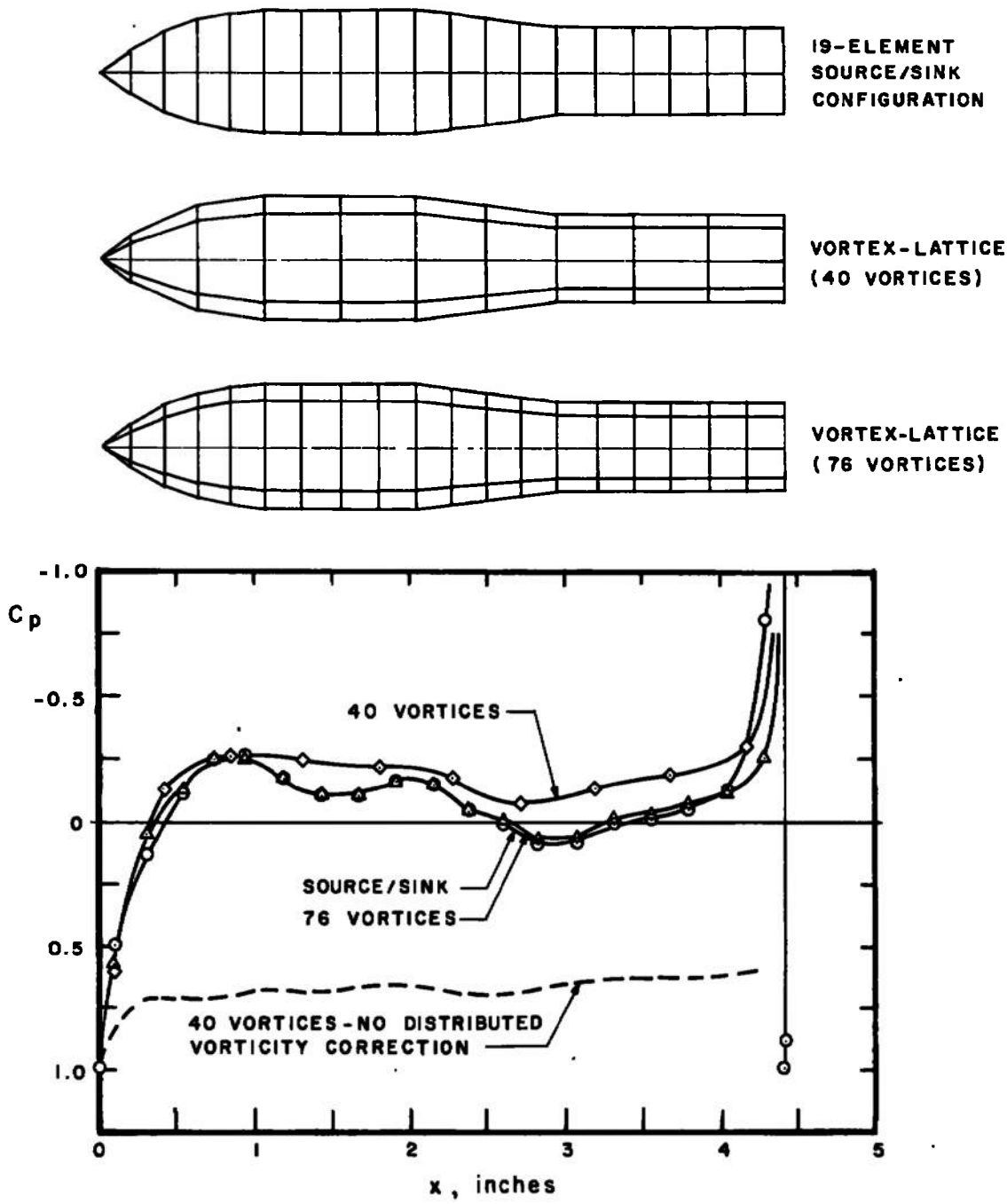


Fig. 9 Comparison of Pressure Distributions on M-117 Bomb Body

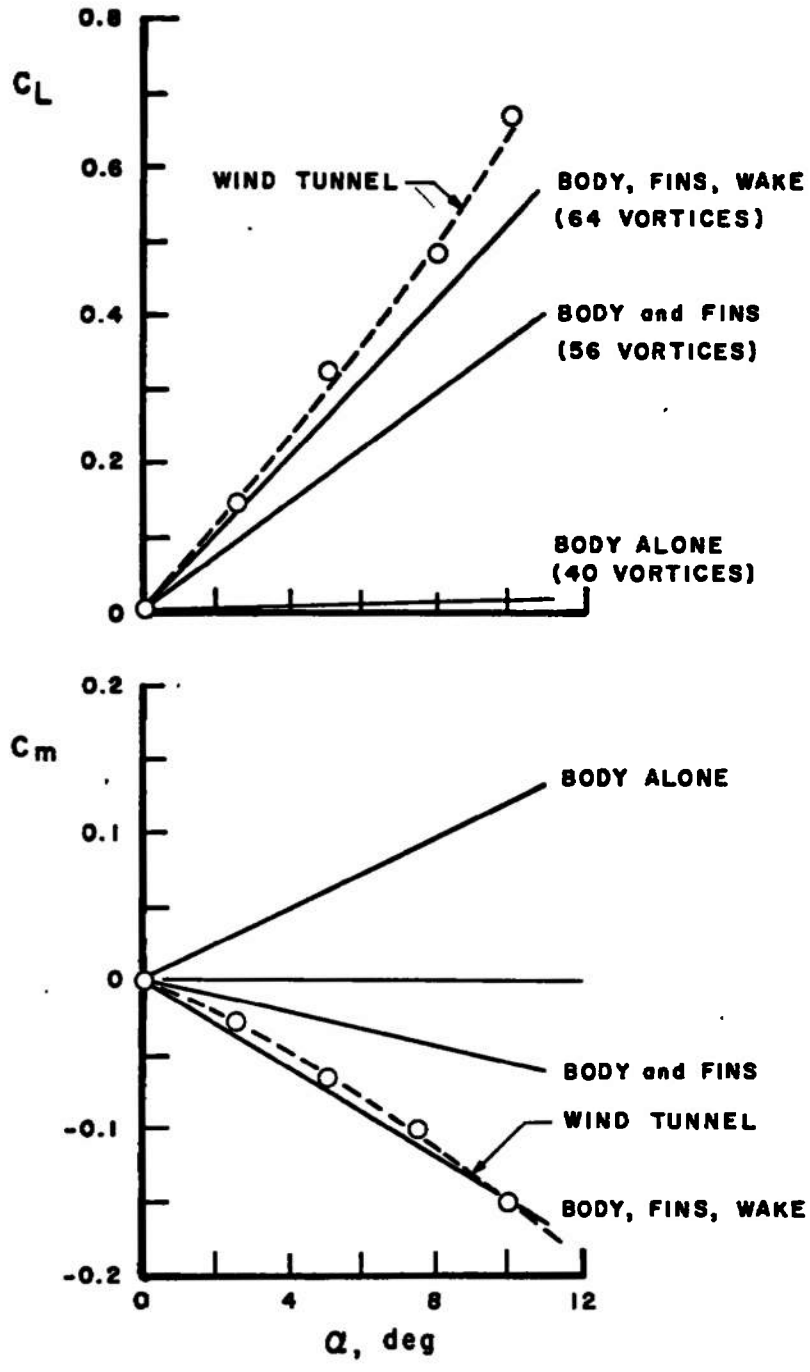


Fig. 10 $C_L$ and $C_m$ on Various M-117 Bomb Vortex Networks

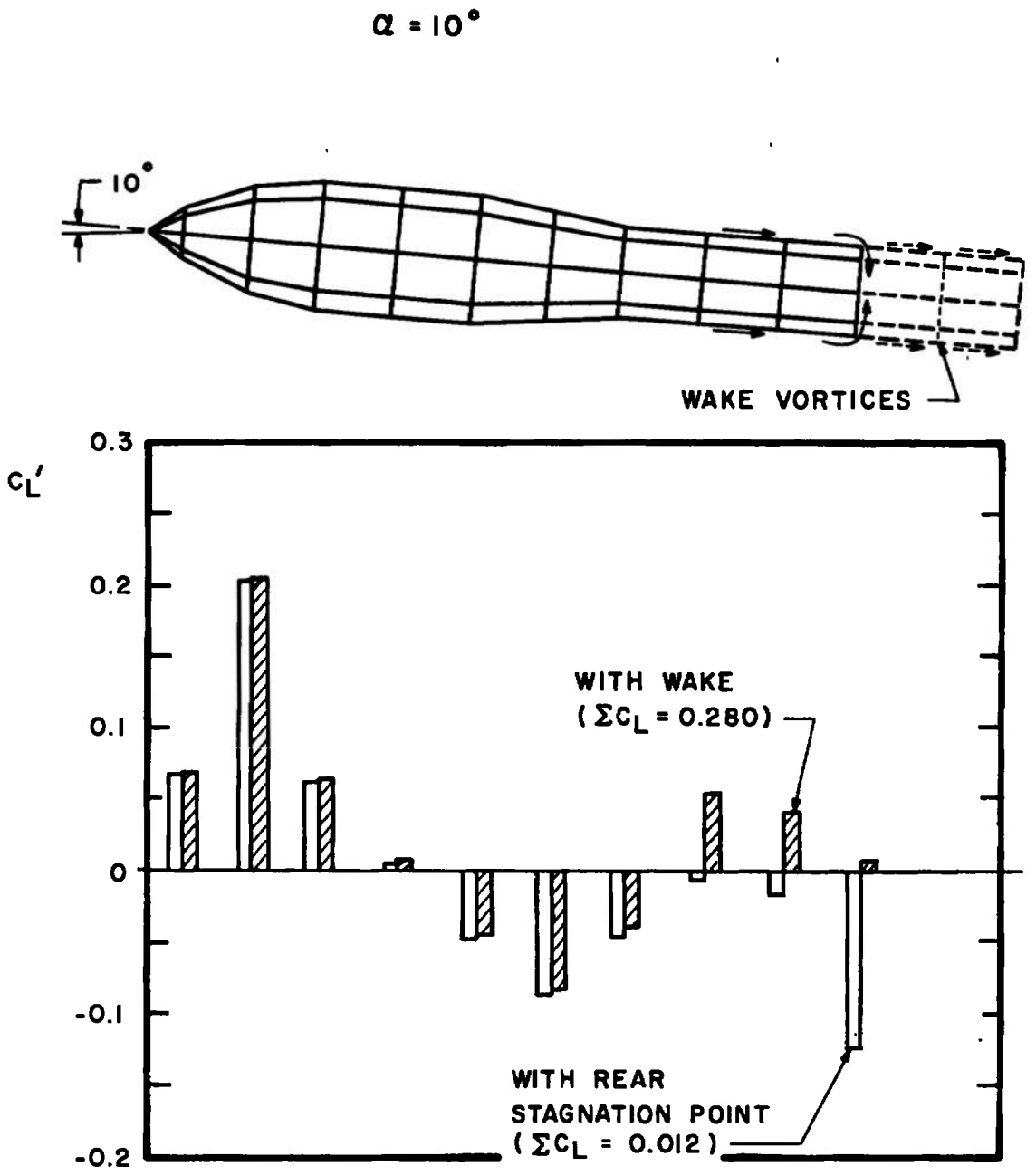


Fig. 11 Lift Distribution on Bomb Body with and without Wake

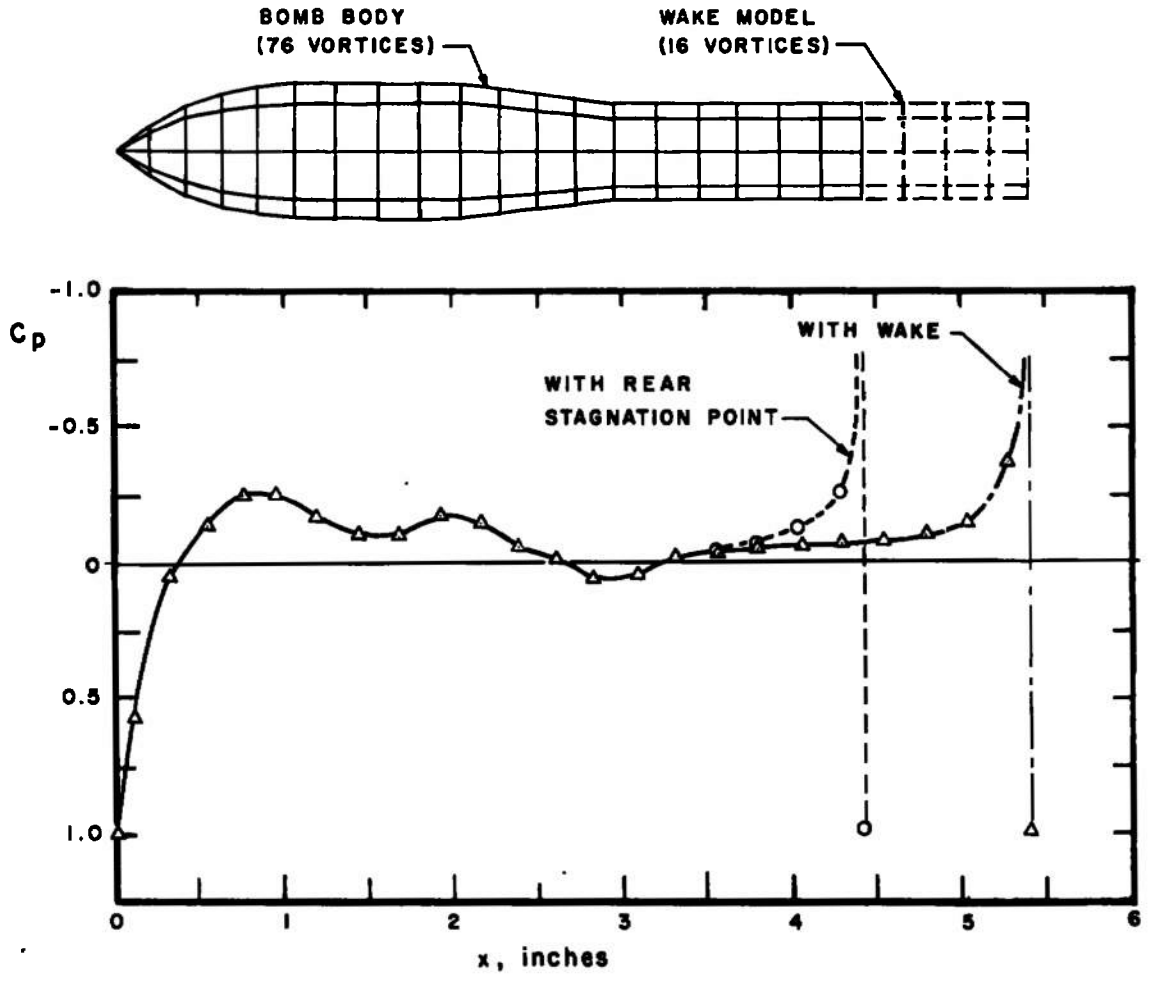


Fig. 12 Pressure Distribution on M-117 Bomb Body with Rear Stagnation Point and with Wake

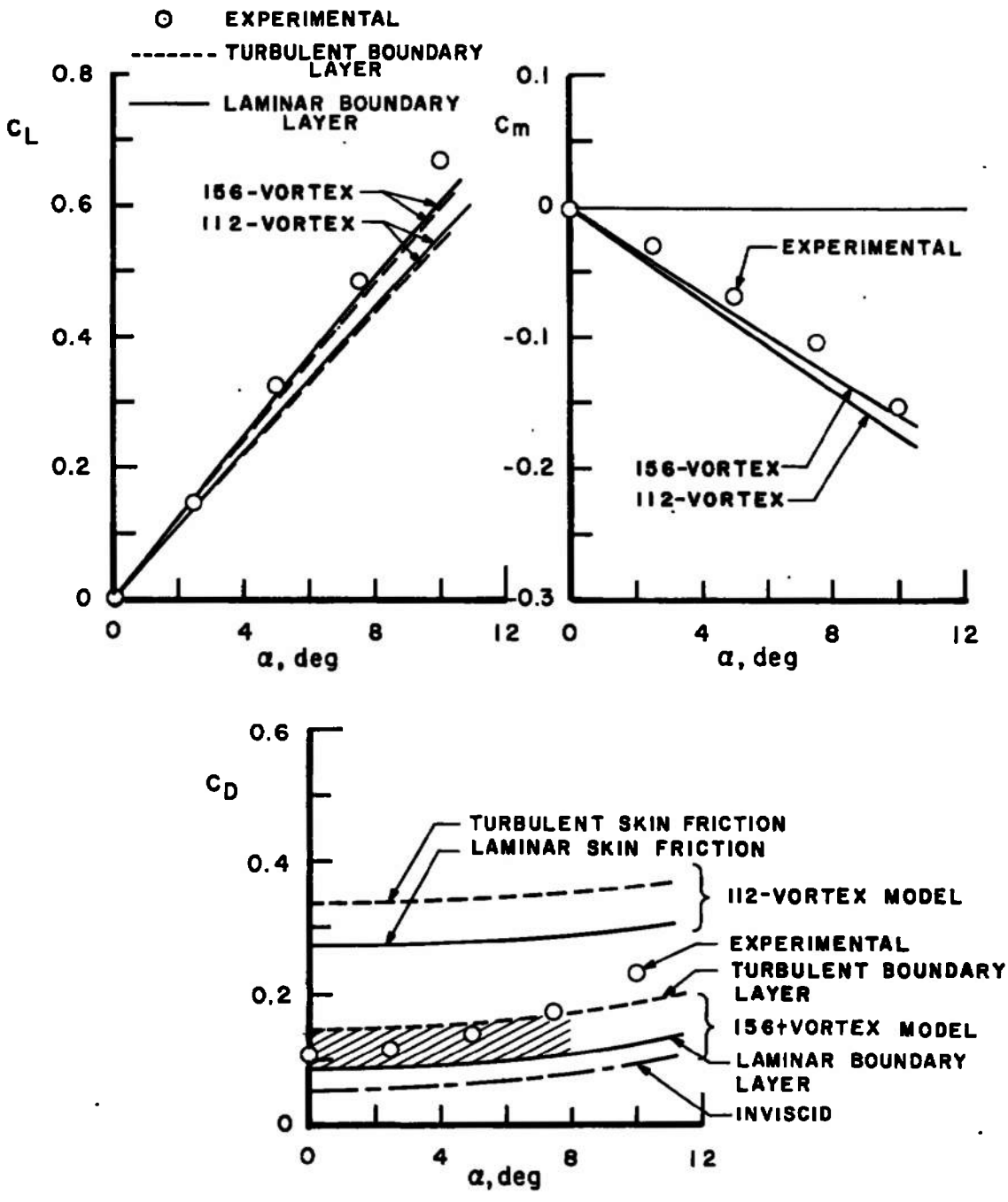


Fig. 13 Comparison of Force and Moment Coefficients for 112- and 156-Vortex Models of M-117 Bomb with Uniform Flow

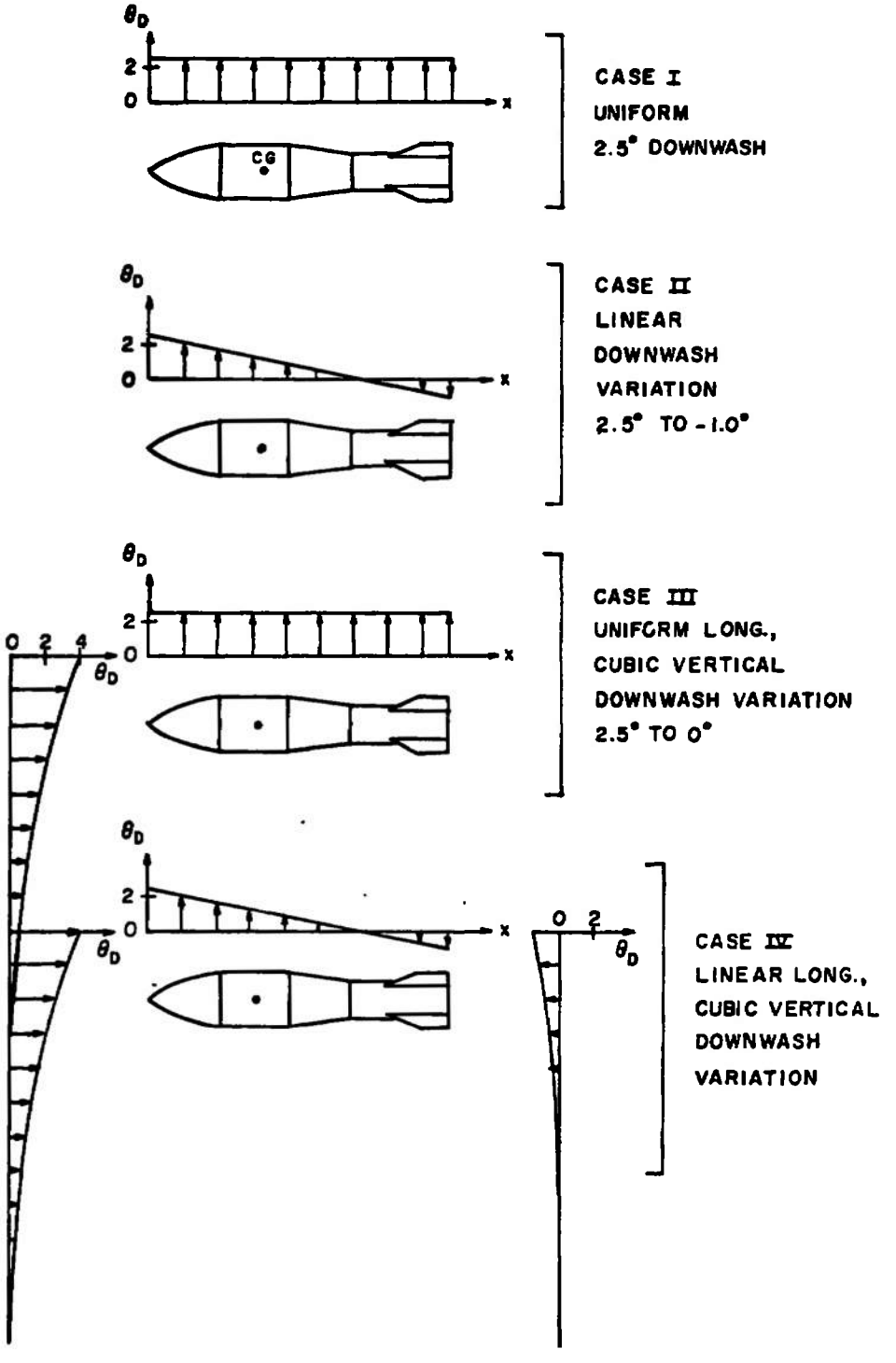


Fig. 14 Idealized Nonuniform Flow Fields

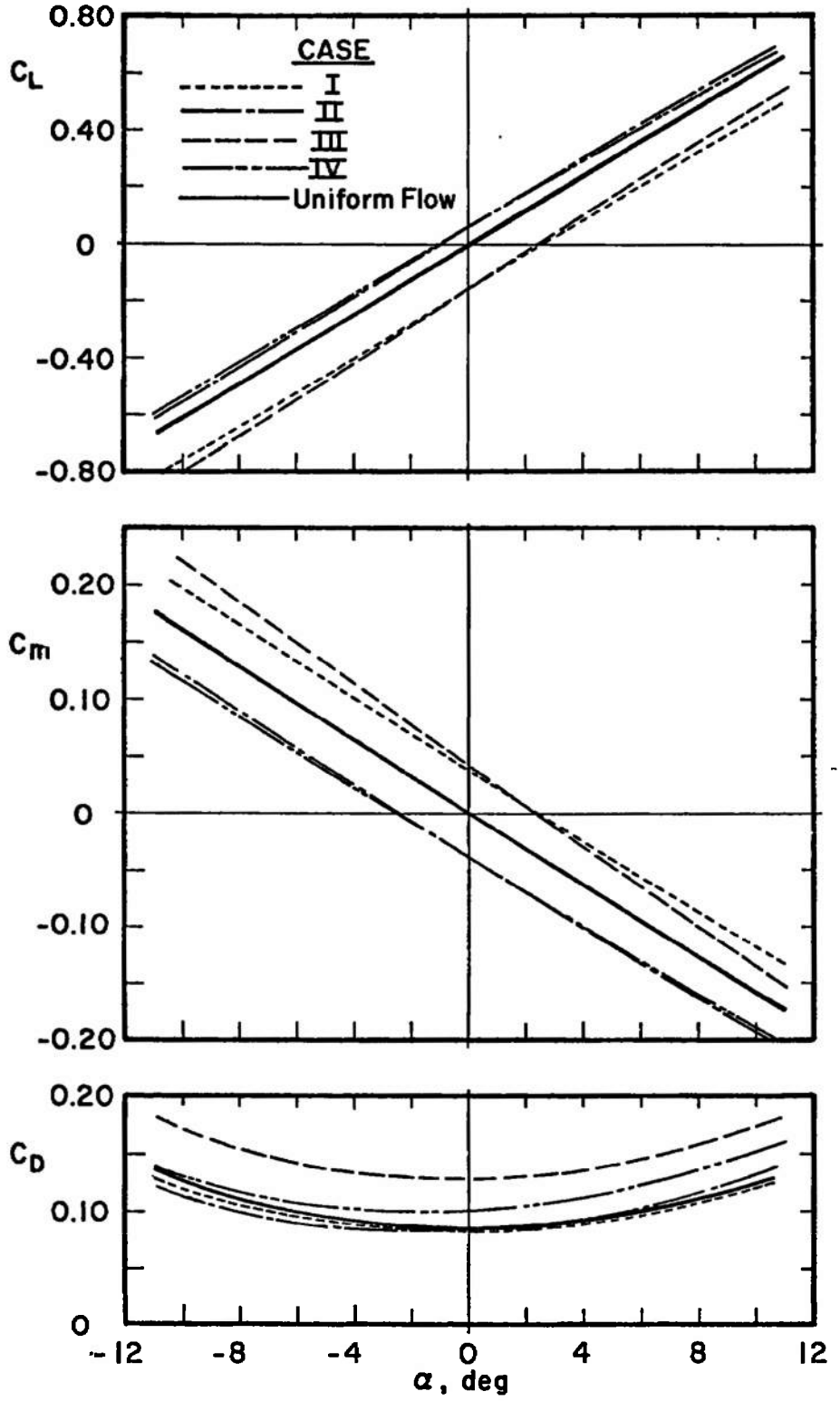


Fig. 15 Calculated Force Coefficients in Idealized Nonuniform Flow Fields

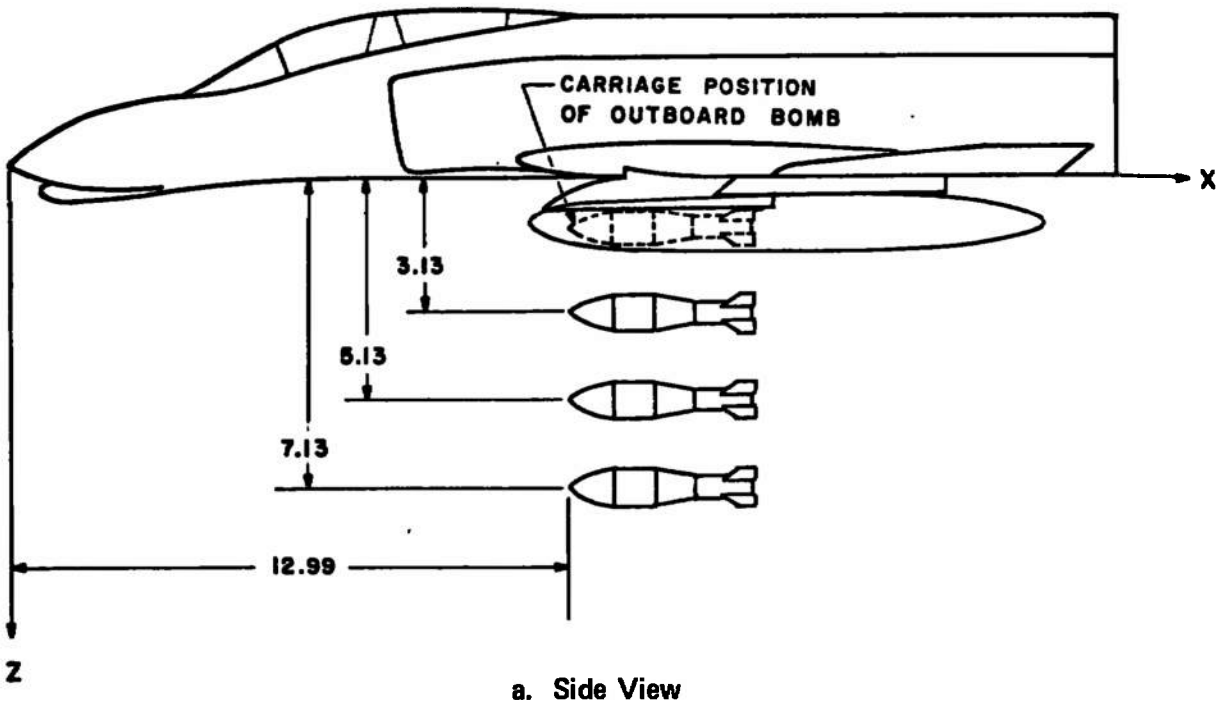


a. Side View

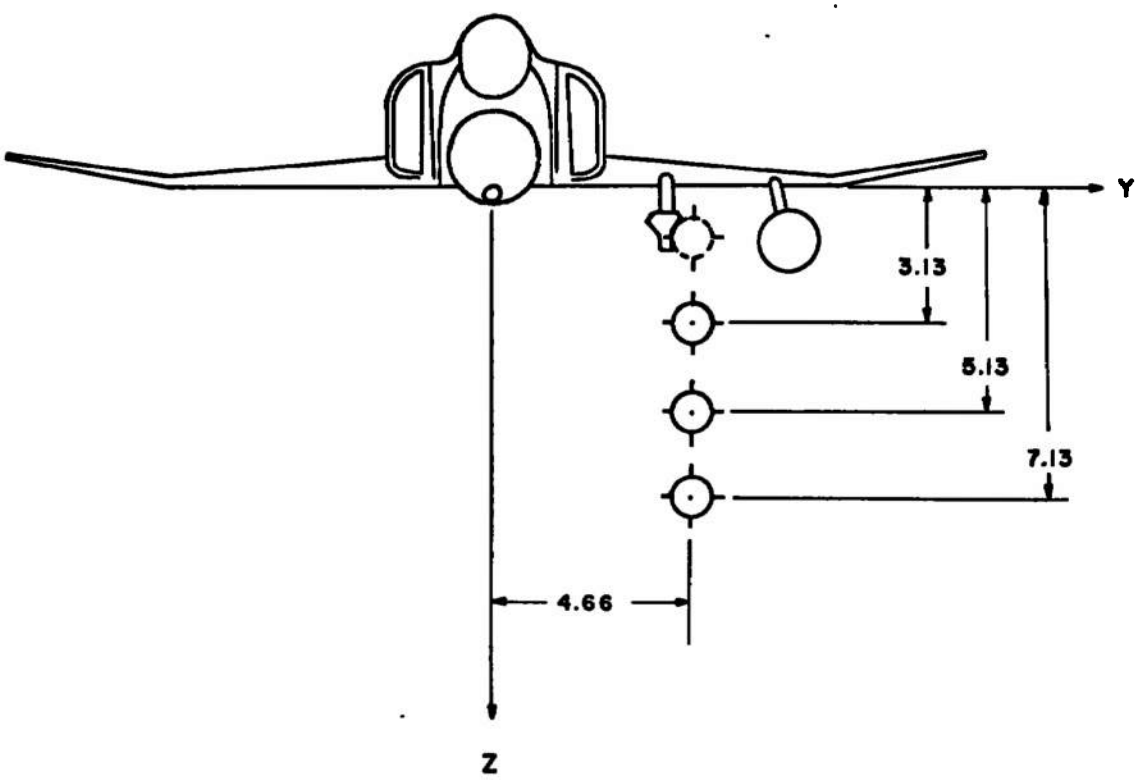


b. Front View

Fig. 16 Locations of M-117 Bomb with Respect to F-4C Parent Aircraft

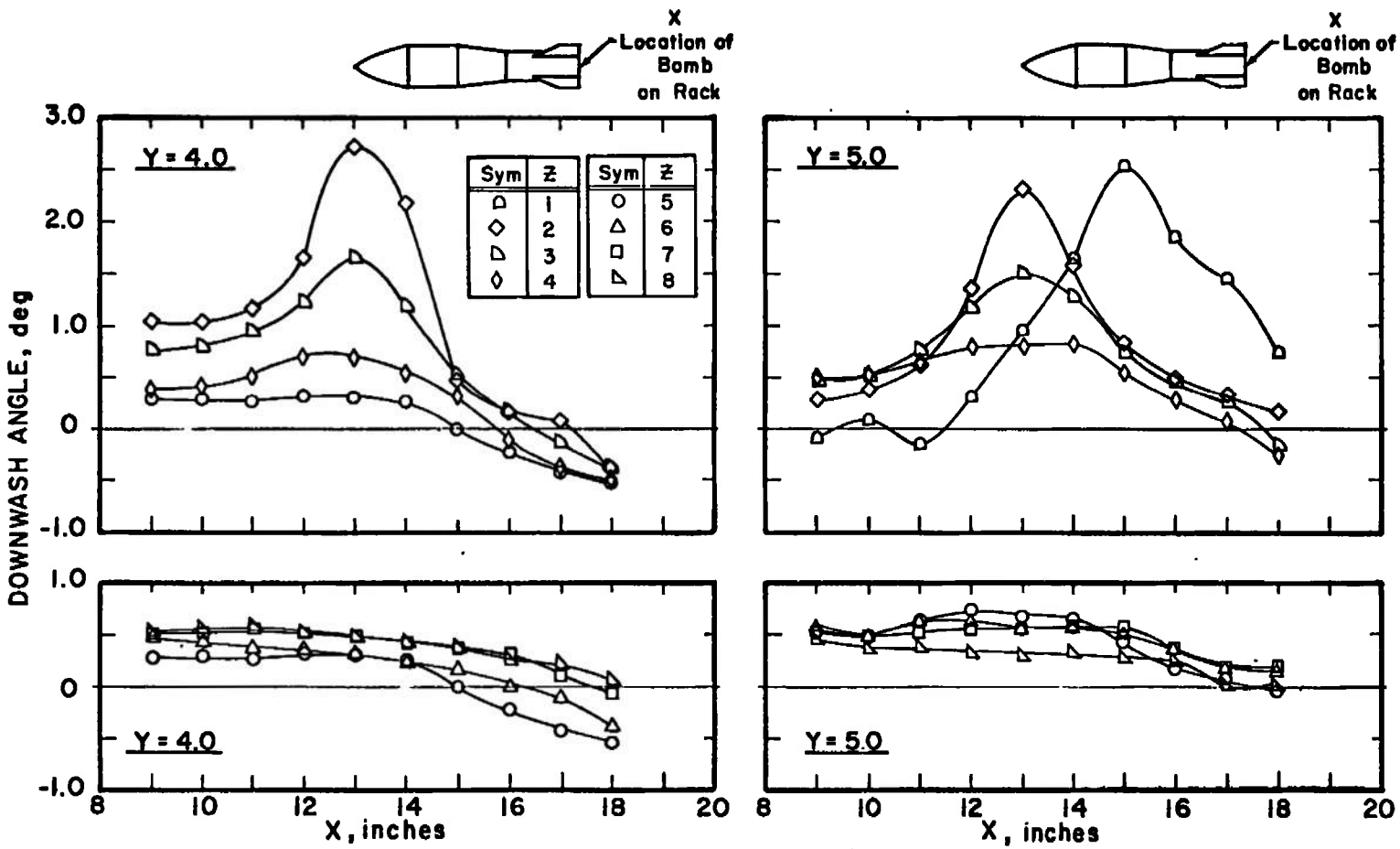


Fig. 17 Downwash Angles beneath F-4C

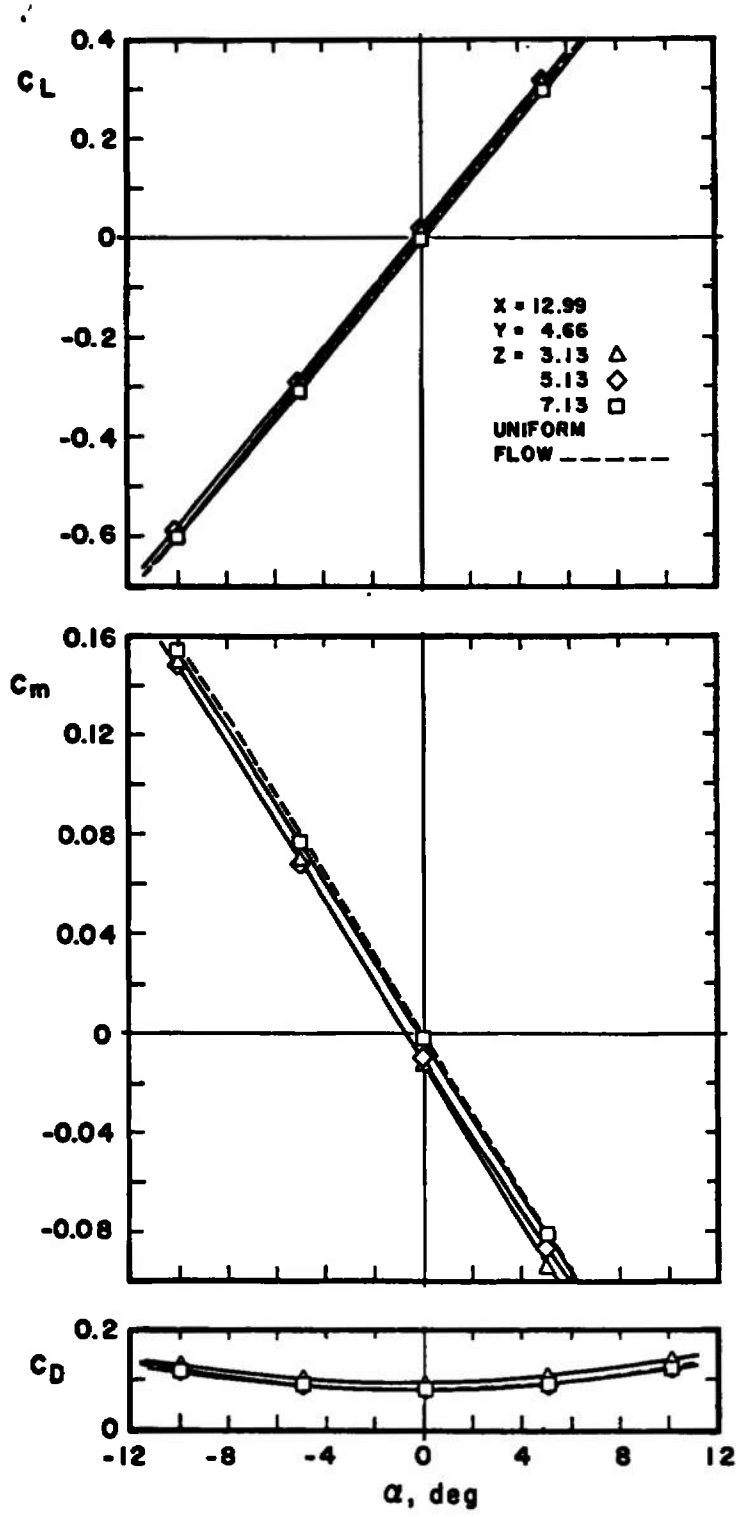


Fig. 18 Calculated $C_L$, $C_m$, and $C_D$ for M-117 Bomb in F-4C Downwash Field for Vertical Displacement of Bomb

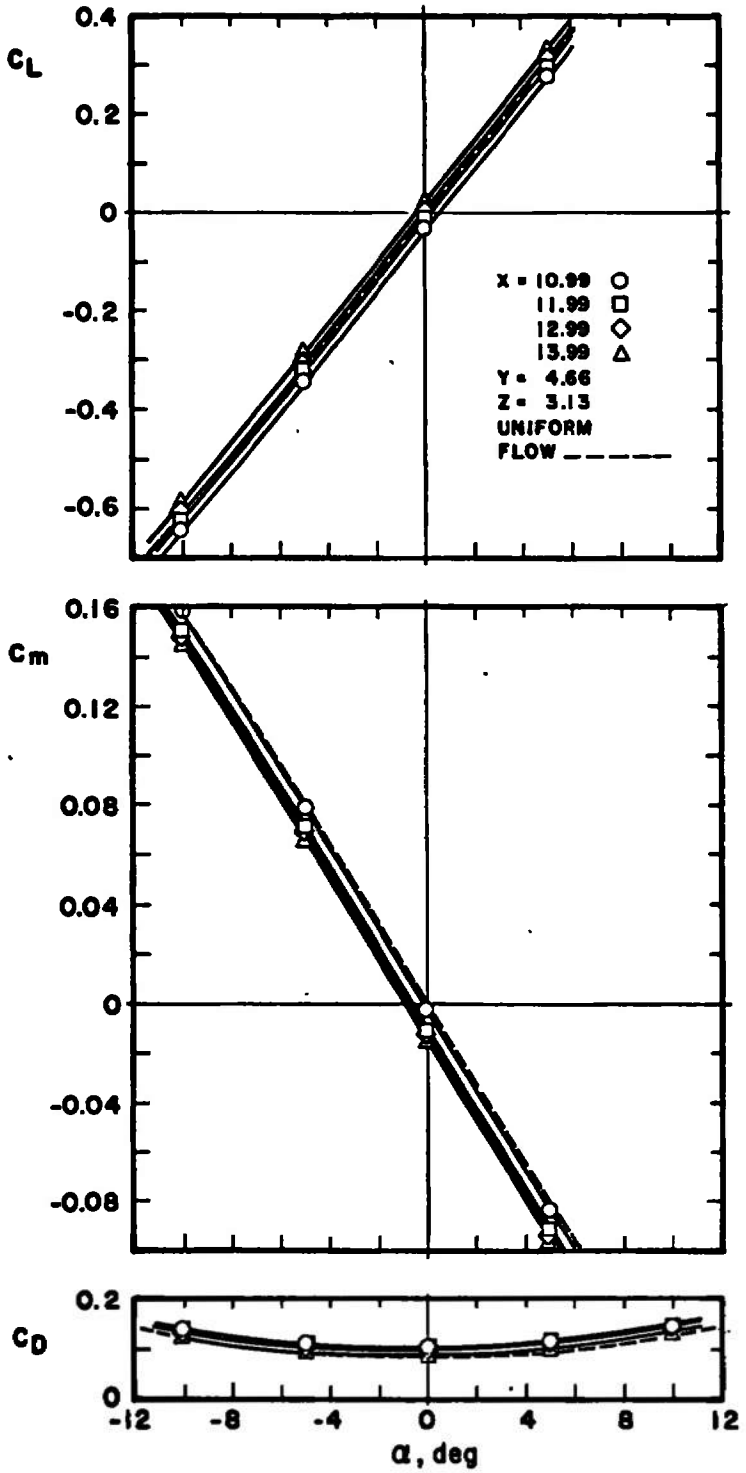


Fig. 19 Calculated $C_L$, $C_m$, and $C_D$ for M-117 Bomb in F-4C Downwash Field for Horizontal Displacement of Bomb

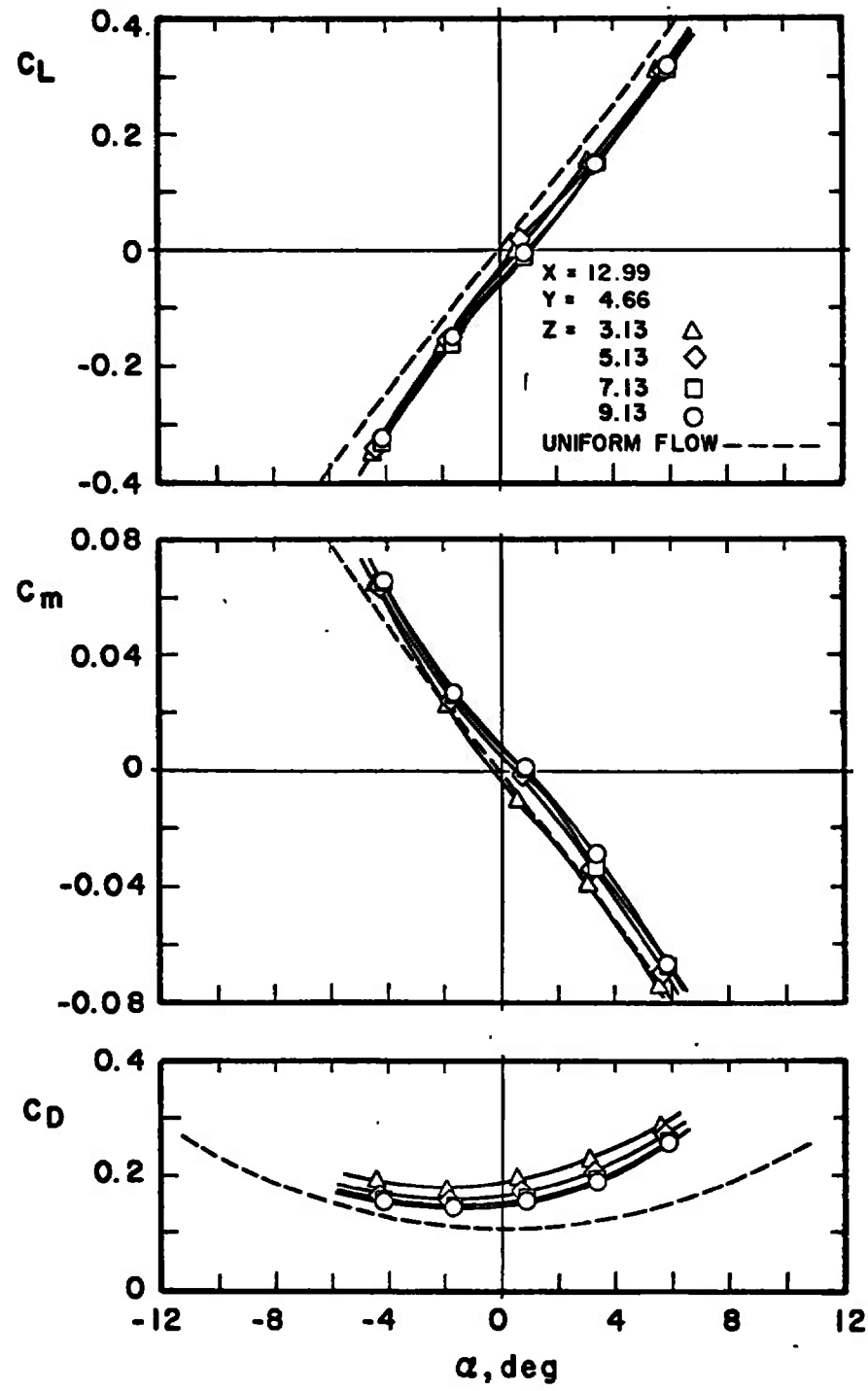


Fig. 20 Experimental $C_L$, $C_m$, and $C_D$ for M-117 Bomb in F-4C Downwash Field for Vertical Displacement of Bomb

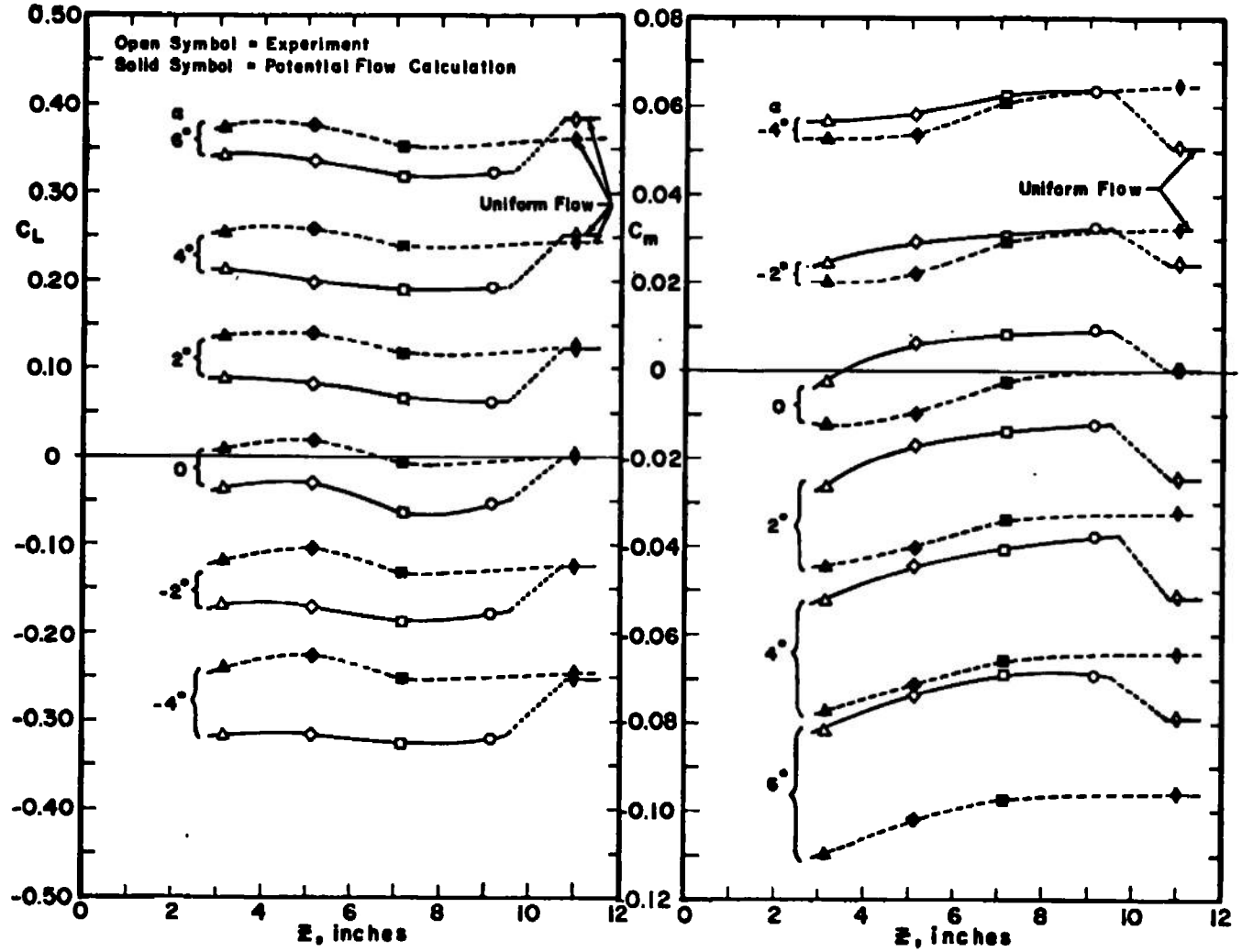


Fig. 21 Experimental and Theoretical Variation of Lift Coefficient with Vertical Position of Bomb beneath F-4C Model

UNCLASSIFIED

Security Classification

**DOCUMENT CONTROL DATA - R & D**

*(Security classification of title, body of abstract and indexing annotation must be entered when the overall report is classified)*

1. ORIGINATING ACTIVITY *(Corporate author)*

Arnold Engineering Development Center
Arnold Air Force Station, Tennessee

2a. REPORT SECURITY CLASSIFICATION

UNCLASSIFIED

2b. GROUP

N/A

3. REPORT TITLE

CALCULATION OF FORCES ON AIRCRAFT STORES LOCATED IN DISTURBED FLOW FIELDS FOR APPLICATION IN STORE SEPARATION PREDICTION

4. DESCRIPTIVE NOTES *(Type of report and inclusive dates)*

Final Report - April 1, 1970, to June 30, 1971

5. AUTHOR(S) *(First name, middle initial, last name)*

W.N. MacDermott and P.W. Johnson, ARO, Inc.

| 6. REPORT DATE | 7a. TOTAL NO. OF PAGES | 7b. NO. OF REFS |
|---|---|---|
| November 1971 | 66 | 8 |

| 8a. CONTRACT OR GRANT NO. | 9a. ORIGINATOR'S REPORT NUMBER(S) |
|---|---|
| b. PROJECT NO. | AEDC-TR-71-186 |
| c. Program Element 63716F<br>d. System 670A | 9b. OTHER REPORT NO(S) *(Any other numbers that may be assigned this report)*<br>ARO-PWT-TR-71-150 |

10 DISTRIBUTION STATEMENT

Approved for public release; distribution unlimited.

| 11. SUPPLEMENTARY NOTES | 12. SPONSORING MILITARY ACTIVITY |
|---|---|
| Available in DDC. | Air Force Armament Laboratory (DLII)<br>Eglin AFB, FL 32542 |

13. ABSTRACT

The aerodynamic characteristics of an M-117 bomb in steady, incompressible, potential flow are computed by representing the bomb planform with a discrete network of vortex singularities. Distribution of velocity and pressure coefficients over the bomb, as well as total force and moment coefficients, are calculated as functions of pitch attitude, the surrounding flow field, and various assumed vortex-lattice modelings. Both spatially uniform and nonuniform flow fields are investigated; the nonuniformities were created by the presence of a parent aircraft. For a properly modeled bomb immersed in a uniform flow, the lift and pitching moment coefficients summed over the entire configuration are found to be within 10 percent of wind tunnel measurements. When the bomb is surrounded by the disturbance flow field produced by an F-4C aircraft, the incremental effects on lift and pitching moment are very similar for theory and experiment.

DD FORM 1 NOV 65 1473

UNCLASSIFIED

Security Classification

| 14. KEY WORDS | LINK A | | LINK B | | LINK C | |
|---|---|---|---|---|---|---|
| | ROLE | WT | ROLE | WT | ROLE | WT |
| mathematical models<br>aerodynamic forces<br>bombs<br>M-117<br>F-4C aircraft<br>aerodynamic characteristics<br>supersonic wind tunnels | | | | | | |